The Influence of Power-Take-Off Control on the Dynamic Response and Power Output of Combined Semi-Submersible Floating Wind Turbine and Point-Absorber Wave Energy Converters

Yulin Si[a], Zheng Chen[a], Weijian Zeng[a], Jili Sun[a], Dahai Zhang[a], Xiandong Ma[b], Peng Qian[a,*]

[a] *Institute of Ocean Engineering and Technology, Ocean College, Zhejiang University, Zhoushan 316021, China*
[b] *Engineering Department, Lancaster University, Lancaster LA1 4YR, UK*

Abstract

Floating offshore wind turbines (FOWTs) have received extensive attention in recent years, particularly after the successful demonstration of several pilot projects, such as Hywind and WindFloat. Integrating wave energy converters (WECs) into FOWTs could potentially help reduce cost of energy by absorbing additional power from waves and introduce restoring moments and extra damping to the floating platform thus reducing motion responses and fatigue loads. In this work, we propose a hybrid floating wind and wave power generation platform, consisting of a semi-submersible FOWT and three point-absorber WECs. Preliminary feasibility study of this concept is performed with verified integrated aero-hydro-servo-mooring numerical simulations. Dynamic response and power output of this hybrid concept are evaluated under several typical environmental conditions. Particularly, different WEC power-take-off control strategies have been comparatively studied, which have shown considerable influences on the platform dynamics and power generation. More specifically, reactive control generally worsen the platform motion responses, while spring-damping control is able to mitigate the pitch motion to certain extent. Regarding power output, reactive control leads to the highest wave power generation, almost twice as much as that of spring-damping, which has been used in most existing works on hybrid power generation system. Moreover, it is found the optimal control design for point-absorber WEC attached to fixed structures is no longer optimal for the combined floating wind and wave energy production platform, which needs further investigations in the future.

Key words: Hybrid power generation platform, semi-submersible, point-absorber, dynamic response, power production, Power-take-off control

*Corresponding author.
Email address: qianpeng18@sina.com (Peng Qian)

1. Introduction

Compared with onshore wind energy, installing wind turbines offshore are widely seen as a more appealing renewable energy solution, as there are vaster available areas, better wind resources, and closer proximity to major demand centres. Offshore wind energy has seen rapid development in recent years, and the cumulative offshore wind capacity has reached 29 GW in 2019 and is expected to arrive at 228 GW in 2030 [1]. Currently, almost all offshore wind turbines are using fix-bottom foundations, mostly monopiles, in shallow waters. While when the water depth exceeds 60 m, floating offshore wind turbines (FOWTs) are considered more economical than fixed-bottom ones [2]. FOWTs have attracted extensive attention from both academia and industry in the past few years, particularly in West and North Europe, North America and East Asia, where suitable shallow water areas for offshore wind farms are limited and deep sea wind resources are abundant. The success of several pilot projects with utility-scale wind turbines mounted on moored floating platforms have demonstrated the feasibility of FOWTs, such as Hywind [3], WindFloat [4] and Floatgen [5]. However, due to the utilization of giant floating support structure and mooring systems, the cost of energy (CoE) for FOWTs is dramatically increased. Moreover, there will be higher structural loads on turbine components due to the extra motion degree of freedom (DoF) of floating platform, which may shorten the fatigue life of critical components and increase the failure risk [6]. To deal with these problems, various approaches have been proposed for FOWT cost reduction and load mitigation. The first category of solutions relies on advanced control for power and load multi-optimization, such as observer-based control [7], individual blade pitch control [8], lidar-assisted control, and structural control [9]. Both power and load can be seen as design objectives in the control synthesis process, but the energy increase is limited and usually there has to be a tradeoff. Besides, it is believed integrating other types of energy harvesting devices into FOWTs could also be a feasible way of reducing CoE, as they produce considerable additional power and share the same infrastructures such as supporting platforms and cables etc. In particular, combining FOWTs with wave energy converters (WECs) have been considered an appealing configuration, as deep sea regions are often with abundant wave energy resources [10], which could contribute to a larger percentage of energy increase. The WECs with proper design might also mitigate FOWT dynamics and loads as they may reduce the wave loads on floating structures or introduce extra restoring moments and positive damping to the system.

Several recent EU funded projects are actively promoting the combined utilization of wind and wave energy, such as MARINA [11], TROPOS [12], MERMAID [13], H2OCEAN [14] and ORECCA [15], and many hybrid concepts have been proposed and studied [16]. In 2011, the research group in UC Berkeley proposed to couple WECs of oscillating water column (OWC) [17], point-absorber [18] and flap types into the WindFloat FOWT [19], which were then named as WindWaveFloat. Preliminary studies on their dynamic behaviours were performed through frequency-domain analysis and scale model wave tank test. Numerical simulation was carried out using WAMIT, a code for calculating

wave loads and motions of offshore structures based on the linear and second-order potential theory [20]. It was stated that most WECs would hardly affect the motions of the WindFloat platform, while the captured wave power was not evaluated since no power take-off (PTO) system was selected. Spar-torus-combination (STC) [21] and Semi-submersible Flap Combination (SFC) [22] are another two floating hybrid wind and wave concepts designed by the research team from Norwegian University of Science and Technology (NTNU). Coupled aero-hydro-servo-elastic dynamic analysis on STC and SFC was performed based on SIMO-TDHMILL3D and SIMO-RIFLEX-AERODYN numerical tools, and the dynamic response, mooring tension and power production were evaluated under both operational and extreme conditions [23]. Experimental study on 1:50 scale models with simple PTO systems was also conducted and compared with numerical results. It was shown these concepts would result in a positive synergy between wind and wave energy generation in terms of power production, while the platform dynamic responses were not much affected by the attached WECs [24]. Other types of hybrid concepts include tention-leg FOWT with three WECs [25], spar FOWT with one wavestar-type WEC [26] or spar FOWT with a torus WEC and two tidal turbines [27], spar-type vertical axis FOWT with a torus-shaped WEC [28], tension-leg [29] or monopile type FOWT with a torus-type WEC [30], semi-submersible platform with two wind turbines and multiple WECs [31], WindFloat FOWT with multiple point-absorber WECs [32], etc. Behaviours of these concepts were assessed with numerical simulations to various fidelities, and some of them had been tested in wave tanks or sea trials. Results again indicated good synergies with respect to power production [33], and several studies also demonstrated platform motion response mitigation effect due to the existence of WECs [34]. Though extensively studied, it was however pointed out in the MARINA project summary report [11] that the low technology-readiness-level (TRL) of WECs and limited additional captured wave power may adversely increase the overall CoE. Therefore, it could be beneficial to adopt proofed WEC models with high TRL, such as WaveStar [35]. At the same time, the WEC PTO control has been demonstrated to have substantial influences on the WEC dynamics and power extraction performances [36]. For instance, the optimal control may give a power increase from 50% to 100% compared to simple linear damping [37]. Consequently, the WEC control systems will also significantly affect the power generation of the hybrid platforms as well as their dynamic behaviours [38]. For example, integrating OWC into the semisubmersible FOWT and applying active control can can both capture the wave energy and help in reducing the motion response [39]. However, almost all existing works only used simple linear passive dampers as PTO systems, which are far from optimal both regarding power production and motion stability. Therefore, the influence of PTO control on the hybrid floating wind and wave platform needs further investigation.

In this study, we propose a hybrid floating wind and wave power generation platform concept, which consists of a 5 MW semi-submersible FOWT and three point-absorber WECs. More specifically, the DeepCwind model is adopted as it is a representative and well-documented semi-submersible FOWT

design. At the same time, three Wavestars are, respectively, attached to the three offset columns of the semi-submersible platform. The Wavestar WEC design is used in this hybrid concept since it is one of the most proofed and close-to-market WEC concepts which has been validated with extensive numerical studies and experimental tests. Under similar naming convention with STC and SFC, the proposed hybrid concept is referred here as the DeepCwind-Wavestar-Combined (DWC). A coupled aero-hydro-servo-mooring dynamic simulation framework within ANSYS-AQWA has been established and verified against FAST [40]. Numerical simulations have been carried out to investigate the feasibility of the DWC design in operational modes. Power production, platform dynamics and mooring load behaviours are assessed under various environmental conditions. Particularly, the influence of WEC PTO control strategies on the DWC power output and dynamic performance is comparatively investigated, which has demonstrated the importance of applying proper PTO control in this hybrid wind-wave power generation platform.

The remainder of this paper is organized as follows: Section 2 presents the detailed design parameters and operational configurations of the DWC concpet. Section 3 describes the established aero-hydro-servo-mooring simulation framework for coupled dynamic analysis of the hybrid platform. Section 4 presents the numerical simulation results and comparatively discusses how PTO control is affecting the motion dynamics, mooring tensions as well as power production of the DWC hybrid platform. The concluding remarks and future research directions are stated in Section 5.

2. The DWC Concept Description

An artistic illustration of the proposed DWC concept is shown in Fig. 1, which consists of a 5 MW DeepCwind semi-submersible FOWT and three point-absorber WaveStar WECs.

- *DeepCwind* is a semi-submersible wind turbine concept developed by the National Renewable Energy Laboratory (NREL) based on Phase II of the Offshore Code Comparison Collaboration Continuation (OC4) project [41]. The semi-submersible platform consisting of several columns is applied for DeepCwind with a main column attached to the tower and three offset columns connected to the main column through a series of pontoons and cross members. The NREL 5 MW baseline wind turbine is supposed to be mounted on the central column. Generator torque control and blade pitch regulation are used for maximum power tracking and power regulation in below and above rated conditions. The blades will be featured in storm protection.

- *Wavestar* is a point-absorber type WEC developed by Aalborg University, which has been one of the most successful WEC models so far with high TRL level. It was firstly proposed in 2003 and has been through various scaled prototypes these years, maturing the concept. The concept consists of a buoy which is fixed to a horizontal shaft through an arm, and the arm rotation drives the hydraulic PTO for power generation. The Wavestar buoy may geometrically be described

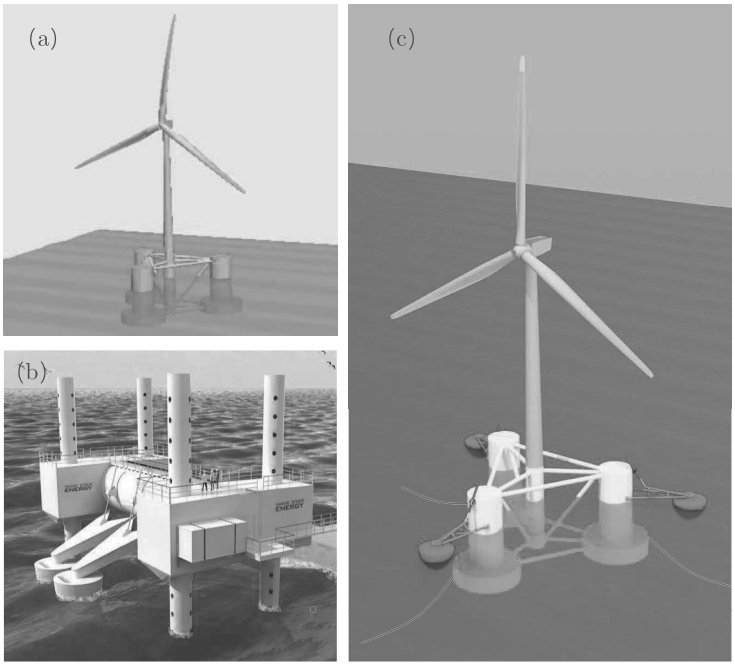

Figure 1: (a) DeepCwind [41], (b) Wavestar [35] and (c) DWC.

as a combination of a sphere with a truncated cone upper part. It is mainly made of glass-fibre and contains a ballast chamber. The chamber is filled with water during power production to lower the natural frequency of the absorber and yield the correct draft of the buoy. For storm protection, the hydraulic cylinders are used for lifting the floats out of water, and the chambers are emptied with an air pressure system.

As an integration of DeepCwind and Wavestars, the hybrid DWC concept is shown in Fig. 1(c), where the added WECs are expected to both produce additional power and improve the floating platform motion dynamics. In the DWC concept, the three point-absorber buoys are, respectively, linked with the three offset columns of DeepCwind platform through connecting arms. A hinged structure is applied between the arm and column, and the relative motion is therefore limited to rotating around the hinged shaft that drives the PTO to produce power. The design consideration of using three centro-symmetrically distributed WECs is the better power quality and smoothness achieved when the waves passes through the system, as the system spans multiple wave lengths. Note that it is also possible to use more than three WECs in the hyrbid platform to increase wave power output, while only three are considered in this work for preliminary feasibility study. Detailed structural design parameters and operational configurations are described below.

2.1. Structural Design Parameters

The structural dimensions of the DWC platform is shown in Fig. 2 and further listed in Table 1, while the inertial properties are listed in Table 2. As shown in Fig. 2, reference point P is defined at the position of the mean sea level (MSL) above the center of gravity (COG) of the platform where the global coordinate system is located. Specifically, WEC 2 is arranged along the x-axis direction. As seen from the figure, the WECs are symmetrically placed at an angle of 120° with 20 m connecting arms. The mooring system is kept the same as DeepCwind with three catenary mooring lines. In order to assist following comparison study, the draft of the DWC platform is kept consistent with DeepCwind when the WECs are operational, i.e. the buoy chambers are filled with water. Note that the mass of one WEC with ballast water only accounts for 0.6% of the DeepCwind weight.

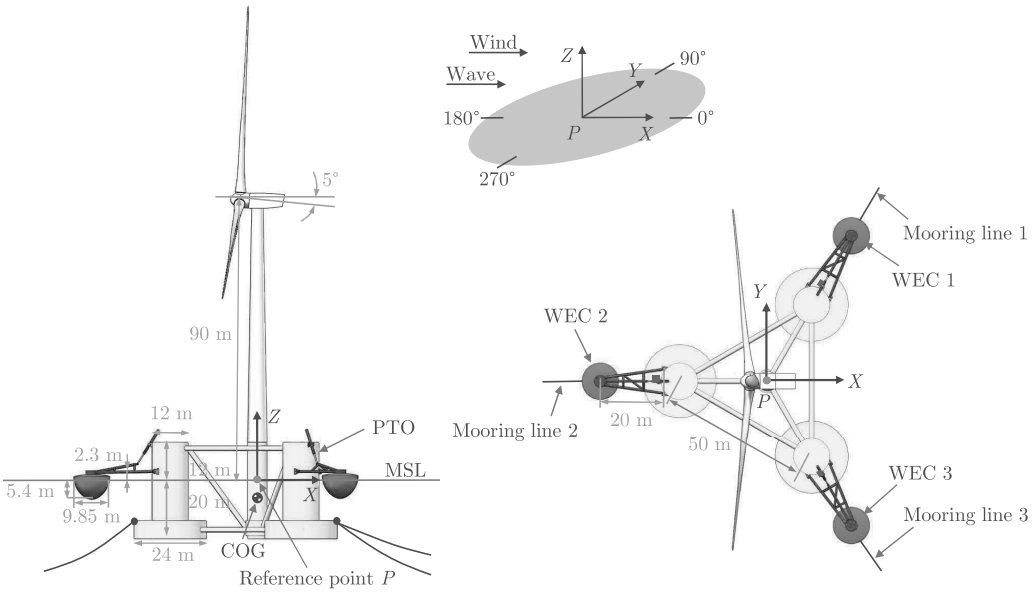

Figure 2: Structural dimensions of the DWC concept.

2.2. Operational Configurations

In this work, the environmental conditions at North Sea are used, as they one of the most suitable sites for FOWTs. For numerical analysis, the wind and wave are correlated based on the simultaneous wind and wave measurements taken between 1973 and 1999 [43], although the joint distribution could be much stochastic and complex. Since waves are wind generated, the mean wind speed v is chosen to be the primary parameter while significant wave height H_s and spectral peak period T_p to be the second and third parameter. Then the joint density distribution function of the characteristic parameters, v, H_s, T_p can be expressed as

$$f_{vH_sT_p}(v, H_s, T_p) = f_v(v) f_{H_s|v}(H_s \mid v) f_{T_p|H_sv}(T_p \mid H_s, v) \tag{1}$$

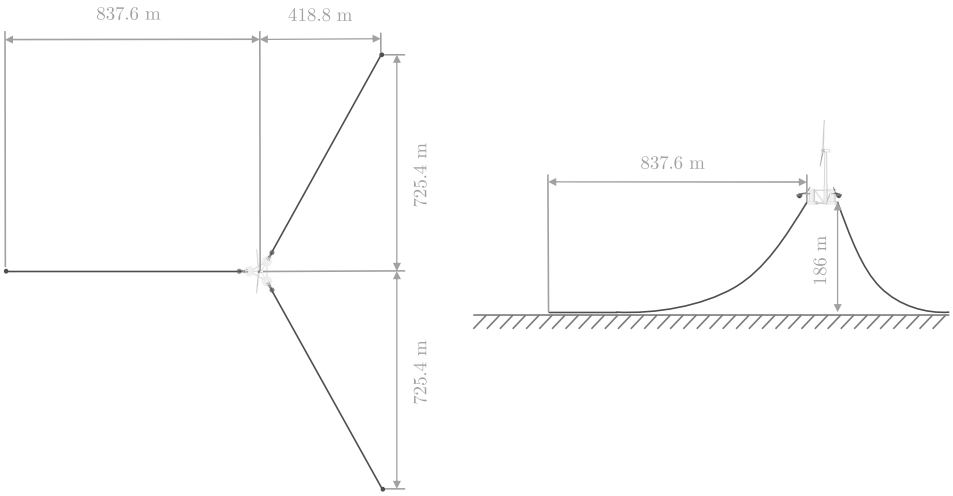

Figure 3: Mooring system dimensions of the DWC concept.

Table 1: Structural dimensions of the DWC concept [41, 42].

	Parameters	Value
Wind Turbine	Rotor diameter	126 m
	Hub diameter	3 m
	Hub height	90 m
	Shaft tilt	5 deg
Platform	Draft	20 m
	Elevation of main column (tower base) above MSL	10 m
	Elevation of offset columns above MSL	12 m
	Spacing between offset columns	50 m
	Length of upper columns	26 m
	Length of base columns	6 m
	Diameter of main column	6.5 m
	Diameter of offset (upper) columns	12 m
	Diameter of base columns	24 m
	Diameter of pontoons and cross braces	1.6 m
WEC	Diameter at free surface	9.85 m
	Draft	5.4 m
	Elevation of WECs above MSL	1 m
	Length of arms	14 m
	Elevation of hinged structures above MSL	2.3 m
Mooring	Depth to anchors below MSL	200 m
	Depth to fairleads below MSL	14 m
	Radius to anchors from platform centerline	837.6 m
	Radius to fairleads from platform centerline	40.868 m
	Unstretched mooring line length	835.5 m
	Mooring line diameter	0.0766 m

Table 2: Inertia properties of the DWC concept [41, 42].

	Parameters	Value
Wind Turbine	Rotor mass	110000 kg
	Nacelle mass	240000 kg
	Tower mass	347460 kg
Platform	Platform mass, including ballast	1.3473×10^7 kg
	CM (center of mass) location below MSL	13.46 m
	Platform roll inertia about CM	6.827×10^9 kg m^2
	Platform pitch inertia about CM	6.827×10^9 kg m^2
	Platform yaw inertia about CM	1.226×10^{10} kg m^2
WEC	Mass (operational)	251000 kg
	Mass (parking)	80000 kg
	CM (center of mass) location below MSL	-1.5 m
	Roll inertia about CM	1.884×10^6 kg m^2
	Pitch inertia about CM	1.884×10^6 kg m^2
	Yaw inertia about CM	2.455×10^6 kg m^2
Moorings	Equivalent mooring line mass density	113.35 kg/m
	Equivalent mooring line mass in water	108.63 kg/m
	Equivalent mooring line extensional stiffness	7.536×10^8 N

The marginal distribution of the mean wind speed can be described by a Weibull distribution with two parameter α and β as

$$F(v) = 1 - \exp\left[-(v/\beta)^{\alpha}\right] \tag{2}$$

where v is the wind speed, α and β is the shape and scale parameter, respectively. Based on the measurements at the Northern North Sea, the method of moments and regression analysis were applied to figure out the value of the parameters. Finally, the expected value of significant wave height H_s with a Weibull distribution and peak period T_p for given wind speed v can be predicted by

$$\begin{aligned} E\left(H_s\right) &= (1.8 + 0.1v^{1.322})\Gamma\left(\frac{1}{2 + 0.135v} + 1\right), \\ E\left(T_p\right) &= \left(4.883 + 2.68H_s^{0.529}\right) \times \left\{1 - 0.19\left[\frac{v - \left(1.764 + 3.426H_s^{0.78}\right)}{1.764 + 3.426H_s^{0.78}}\right]\right\}, \end{aligned} \tag{3}$$

and the correlationship is plotted in Fig. 4. More details of the joint distribution model can be found in [43]. According to the correlated environmental conditions, power curve for the WECs could be also predicted.

The NREL 5 MW baseline wind turbine uses a conventional variable-speed, variable blade-pitch-to-feather control system. However, the baseline controller for fixed bottom wind turbine may introduce negative damping for the FOWT that may lead to large resonant motions. Therefore, control modifications were made for DeepCwind included a reduction of gains in the blade pitch system and a change in the generator-torque control strategy when operating at rated power. Its power curve is marked

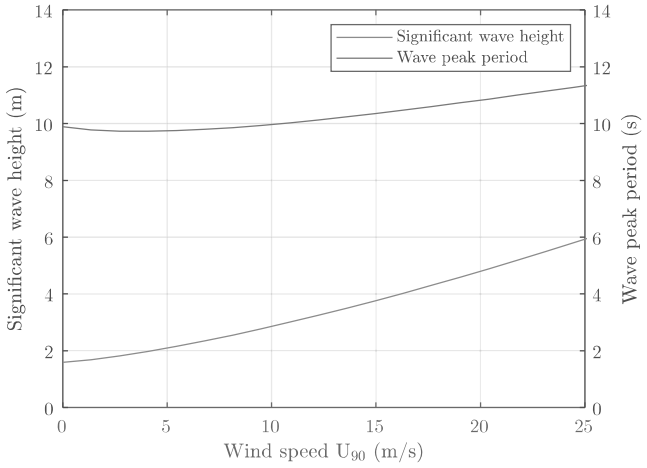

Figure 4: Significant wave height and peak period with given wind speed for a fully developed sea with JONSWAP spectrum.

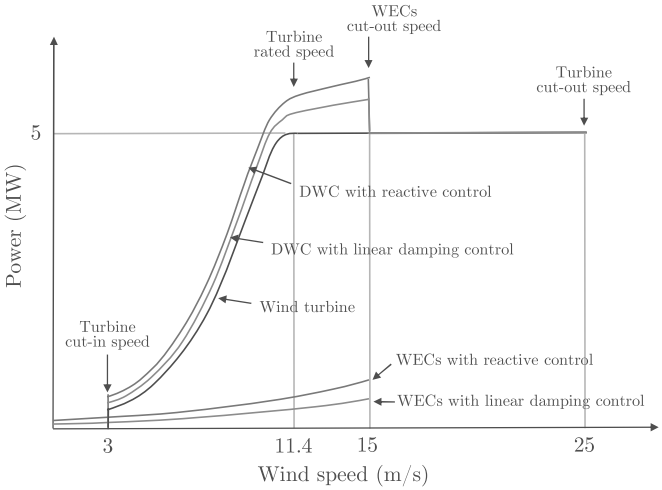

Figure 5: Power curve of the DWC concept.

with black color in Fig. 5, where the cut-in, rated and cut out wind speed are 3 m/s, 11.3 m/s and 25 m/s, respectively. Wavestar WECs also have an operational range. In this work, the WECs are designed to produce power within the significant wave height of 0.5 m - 3.5 m. When H_s exceeds the designed 3.5 m threshold, the ballast water will be emptied and buoys will be lifted out of the water by hydraulic cylinders for protection as illustrated in Fig. 6, so the wave power production only happens within the designed wave range. Estimated power curves for WECs are also plotted in Fig. 5. Note that the WEC power output is highly depending on PTO control strategies [35], which can be also noticed by the difference between the WEC power curves under reactive control and linear damping control [44]. Their influences on the platform dynamics and power output will be further investigated with numerical simulations.

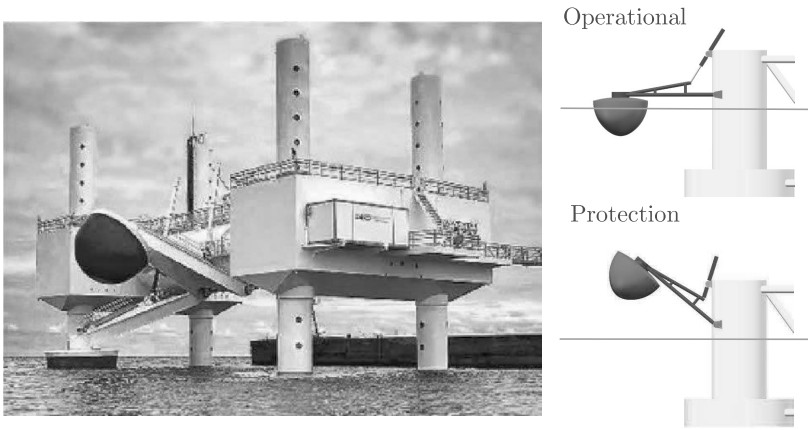

Figure 6: Wavestar prototype operational and protection modes.

3. Aero-Hydro-Servo-Mooring Simulation Framework

In this section, the established aero-hydro-servo-mooring simulation framework for coupled dynamic analysis of the hybrid platform is introduced. Though within quite similar physical domains, numerical simulation tools for FOWTs and WECs are usually different, as they have distinct motion DoFs and environmental loadings. This makes it difficult to perform integrated time-domain analysis for the hybrid floating platform within the same framework. Numerical simulations in previous works were carried out either by only investigating frequency-domain behaviours using WAMIT [19] or by coupling FOWT and WEC simulation modules together, for instance SIMO-TDHMILL3D [45], SIMO-RIFLEX-AERODYN [25], HAWC2-WAMSIM [46]. Due to the accessibility, we establish the integrated DWC simulation framework within one environment ANSYS-AQWA [47], which has been widely used in marine structure design and analysis, such as offshore renewable energy devices. AQWA provides an integrated environment for multi-body dynamic analysis and hydrodynamic and mooring load calculations. Additionally, aerodynamic loads as well as control actuations could be incorporated through user-defined functions, which will make a coupled aero-hydro-servo-mooring numerical simulation analysis possible. The simulation workflow of the hyrbid floating wind and wave platform within AQWA is shown in Fig. 7. Note that the elasticity of wind turbine blades and tower are not considered here due to the limitation of model capability. Below, each module within this framework is explained in detail, and the motion equation for DWC multi-body dynamics, as well as loading calculations from aerodynamics, hydrodynamics, mooring, and PTO control strategies are described, respectively.

3.1. Multi-body dynamic motion

As mentioned above, in this work we treat the wind turbine structures as rigid bodies, i.e. the rotor-nacelle-assembly (RNA) and the tower. The wind turbine dynamics such as rotor and drivetrain rotations are not numerically modelled as motion DoFs. Besides, the three WECs are also seen as

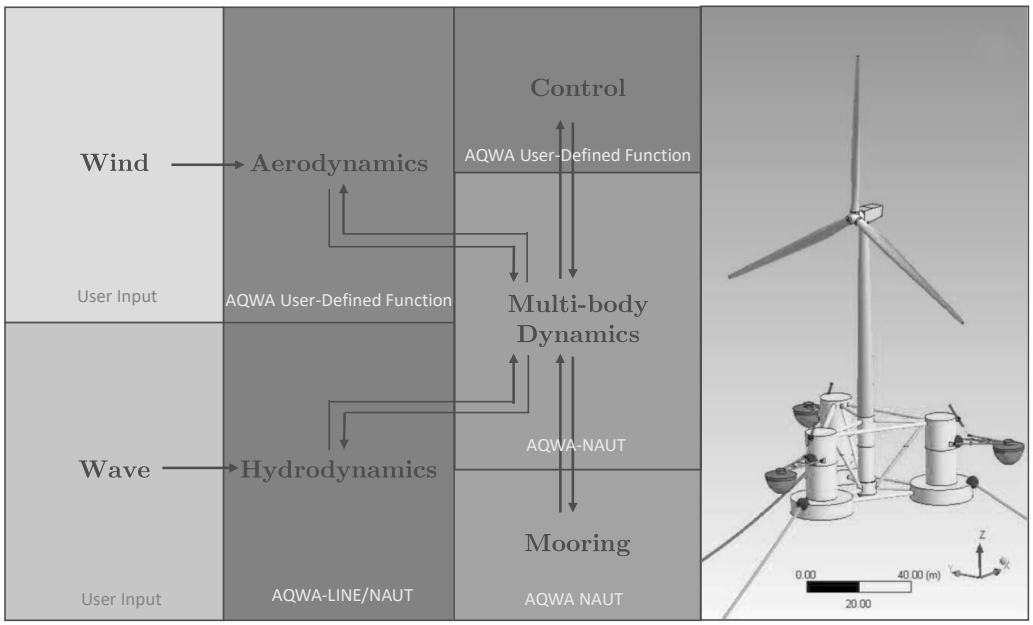

Figure 7: Aero-hydro-servo-mooring coupled simulation framework.

rigid and can only rotate around the pivot point. Therefore, the DWC model has 9 DoFs in total with 6 motion DOFs for FOWT and 3 rotational DOFs for WECs, and the motion equation of the DWC model can be then written into the following form based on Cummins theory [48],

$$\begin{bmatrix} M^D + A^D(\infty) & A^{DW}(\infty) \\ A^{WD}(\infty) & M^W + A^W(\infty) \end{bmatrix} \begin{bmatrix} \ddot{X}^D \\ \ddot{X}^W \end{bmatrix} = \begin{bmatrix} F^D_{aero} + F^D_{hydro} + F^D_{buoy} + F^D_{grav} + F^D_{moor} - F^W_{PTO} + F^D_W \\ F^W_{hydro} + F^D_{buoy} + F^W_{grav} + F^W_{PTO} + F^W_D \end{bmatrix} \tag{4}$$

where the superscripts D and W represent DeepCwind and Wavestar, respectively. M is the mass, and $A(\infty)$ is the hydrodynamic added mass matrix at infinite high frequencies, where the hydrodynamic interactions between the semi-submersible platform and the WECs are also included. $\ddot{X}$ is the (translational and rotational) acceleration vector. External loads of forces and torques come from aerodynamics F_{aero}, hydrodynamics F_{hydro}, hydro-static buoyancies F_{buoy}, gravitation F_{grav}, mooring F_{moor}, PTO of WECs F_{PTO}, and hinge connection interactions F^D_W and F^W_D, where $F^D_W = -F^W_D$.

3.2. Aerodynamic Loads

The aerodynamic loads imposed on the rotor are affected by many factors, such as wind speed and direction, blade pitch angle, platform motion and blade elasticity [49]. In modern wind turbine design tools, blade element momentum (BEM) theory is usually the numerical basis for aerodynamic calculation [50], in which the blades are divided into a number of independent sections along the length, and sectional lift and drags are evaluated and integrated into the overall thrust and torque. Besides, the calculation also requires the information about control actuation, blade elasticity and tower top motion, which will affect the relative wind speed experienced by the blades. Therefore, aerodynamic

calculation is usually a coupled and complex process. More simply, another approach for concept study is to use steady-state loads of rotor thrust and torque, which is usually applicable for modelling the aerodynamic loads of fixed-bottom wind turbines. It has shown improved computational efficiency with decent accuracy as well [51]. With this approximation, the nominal control operation, i.e. maximum power tracking and blade pitch regulation, has already been incorporated into the operational curves.

However, the floating platform induced tower top motion for FOWTs is also a decisive factor for aerodynamic load calculation, as it becomes more significant for FOWTs than fixed bottom ones and will strongly affect the relative wind speed passing the blades. Therefore, the aerodynamic loads are further augmented in this work with the tower top motion to better characterise the transient aerodynamic behaviours. This is achieved by surface fitting the FAST simulation results under a continuous set of wind speeds and irregular waves, so that transient processes could be also incorporated in the modelling process. In the surface fitting process, the nacelle motion velocity and wind velocity along the axial direction of the main shaft, v_{nac}^{sft} and v_{wnd}^{sft}, are seen as two independent variables, and they can be quantified, respectively, as

$$\begin{aligned} v_{nac}^{sft} &= v_{sg}\cos(\theta_p + \theta_{tilt}) + \dot{\theta}_p L\cos\theta_{tilt} - v_{hv}\sin(\theta_p + \theta_{tilt}), \\ v_{wnd}^{sft} &= v_{wnd}\cos(\theta_p + \theta_{tilt}), \end{aligned} \tag{5}$$

where v_{wnd} denotes the instantaneous horizontal wind speed at hub height, v_{sg} and v_{hv} are, respectively, the surge and heave velocity with regards to FAST wind turbine reference point, θ_p is the pitch angle of the floating platform, L represents the distance between hub height and the reference point P, and θ_{tilt} is the 5° main shaft tilt angle. It is shown the aerodynamic thrust f and torque τ with polynomial fitting in the following form could produce R-squared values of above 98%.

$$\begin{aligned} f &= a_4 {v_{wnd}^{sft}}^2 + a_3 v_{wnd}^{sft} v_{nac}^{sft} + a_2 v_{wnd}^{sft} + a_1 v_{nac}^{sft} + a_0, \\ \tau &= b_6 {v_{wnd}^{sft}}^3 + b_5 {v_{wnd}^{sft}}^2 v_{nac}^{sft} + b_4 {v_{nac}^{sft}}^2 + b_3 v_{wnd}^{sft} v_{nac}^{sft} + b_2 v_{wnd}^{sft} + b_1 v_{nac}^{sft} + b_0, \end{aligned} \tag{6}$$

where a_0, ..., a_4, b_0, ..., b_6 are the polynomial coefficients. The fitting results for the transient responses are illustrated in Fig. 8, also showing good agreement between the aero-elastic code and the proposed model. The obtained aerodynamic load model is then implemented as a user-defined function in the AQWA time-domain simulation.

3.3. Hydrodynamic loads

For both FOWTs and WECs, potential flow theory is commonly used as it yields an adequate description of wave-structure interactions in moderate wave conditions. There have been several widely used three-dimensional potential flow solvers (e.g. WAMIT [20], AQWA [47], and NEMOH [52]). They are able to solve the Laplace equation for the velocity potential, which assume the flow is inviscid, incompressible, and irrotational. More details about potential flow theory can be found in [20], which are not further described here for brevity.

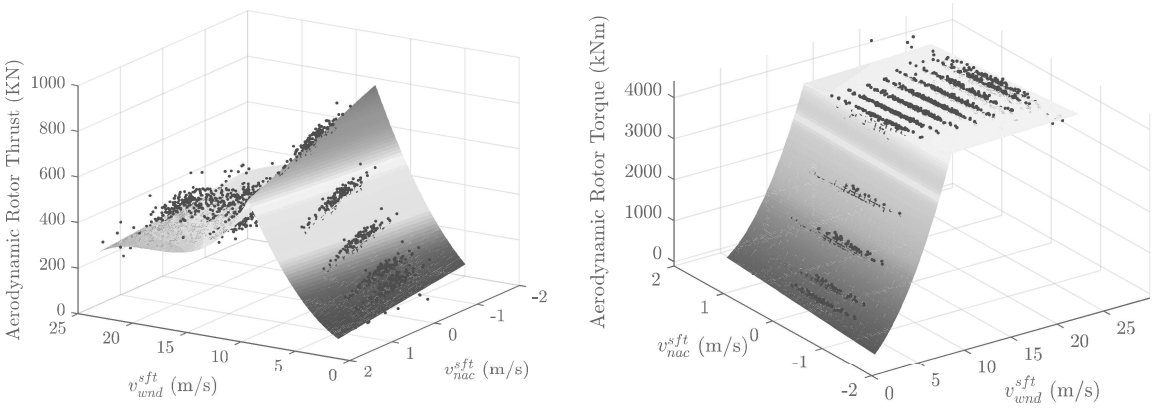

(a) Aerodynamic rotor thrust fitting.

(b) Aerodynamic rotor torque fitting.

Figure 8: Aerodynamic loads surface fitting results.

As a modularised and fully integrated hydrodynamic analysis suite, AQWA is used in this work for hydrodynamic analysis. It is based on panel method and employs three-dimensional potential flow theory in the frequency domain to solve hydrodynamic radiation and diffraction coefficients, and then solves marine structure motion equations, e.g. Equation (4), to obtain hydrodynamic response in time-domain. The AQWA generated mesh for the DWC platform is shown in Fig. 9. And the mesh quality is analyzed to meet the requirements of mesh independence. The calculated frequency-dependent hydrodynamic loads $F_{hydro}(\omega)$ based on potential flow theory mainly comprise wave radiation (added mass $A(\omega)\ddot{X}$ and radiation damping $F_{rad}(\omega)$) and wave diffraction (incident wave loads $F_{inc}(\omega)$). Note that the viscous damping is not included in potential flow methods, while the flow-separation-induced viscous drag cannot be ignored for the semi-submersible platform as mentioned in [41]. Therefore, additional Morison hull drag terms have to be further augmented in AQWA in order to account for hydrodynamic loads of the pontoons and cross members that connect the columns, as their diameter is much smaller than the wavelength. The extra drag accounted for neglected damping in potential flow theory can be represented as

$$F^i_{drag}\left(\dot{X}^j\right) = -C^{ij}\left|\dot{X}^j\right|\dot{X}^j. \tag{7}$$

where C^{ij} is the (i,j) component of the extra additional drag matrix and X^j is the first derivative relative to time of the j^{th} DoF of the platform [41]. Moreover, multi-body hydrodynamic interactions between the semi-submersible platform and WEC buoys can be also characterized within AQWA hydrodynamic analysis framework [47]. The hydrodynamic interaction includes not only the radiation coupling but also the shielding effects as well, which are important for the WEC buoys and semi-submersible columns. Extended hydrodynamic coefficient matrices are needed to account for multi-body hydrodynamic interactions. In the DWC case, the total unsteady potential for the six DoFs of

the four rigid bodies can be expressed as a superposition

$$\varphi\left(\overrightarrow{X}\right)e^{-i\omega t}=\left(\varphi_I+\varphi_d+\sum_{n=1}^{4}\sum_{j=1}^{6}\varphi_{rnj}X_{nj}\right)e^{-i\omega t} \tag{8}$$

where $\overrightarrow{X}$ the coordinates of the panel center, φ_I is the isolated space dependent incident, φ_d is the diffraction potential, φ_{rnj} is the radiation potential of the j^{th} DoF motion of the n^{th} body and the X_{nj} is the amplitude of the j^{th} DOF motion of the n^{th} body. Once the unsteady potential is calculated, the wave exciting forces and radiation force related added mass and damping coefficients are expressed as

$$\begin{aligned}&F_{jn}=F_{Ijn}+F_{djn}=-i\omega\rho\int_{S_{0n}}\left[\varphi_I+\varphi_d\right]m_{jn}dS\\&A_{jn,km}+\tfrac{i}{\omega}B_{jn,km}=-\tfrac{i\rho}{\omega}\int_{S_{0n}}\varphi_{rkm}m_{jn}dS\end{aligned} \tag{9}$$

where m, n correspond to the m-th and n-th structures, j, k correspond to the motion DoFs, A is the added mass, B is the damping coefficient, S_{0n} is the mean wetted hull surface of the n-th structure [47].

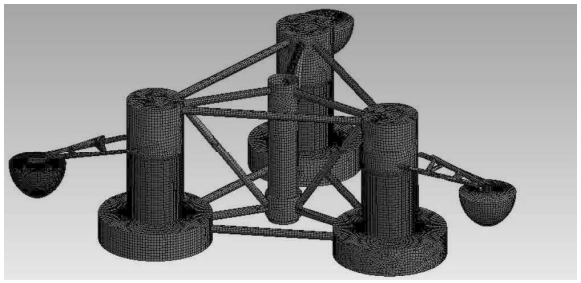

Figure 9: AQWA generated mesh of the DWC platform and WECs.

To sum up, the calculated hydrodynamic loads for the DWC hybrid platform include added mass effect, radiation damping, incident wave loads, viscous drag and multi-body hydrodynamic interactions.

3.4. Power Take-Off System

As shown in Fig. 10, the PTO systems of oscillating body WECs either use mechanical or hydraulic transmissions to power conventional high speed rotational generators or install special designed linear generators for direct drive. The 110 kW Wavestar prototype tested at the west coast of Denmark has two buoys, and each of them is equipped with a hydraulic PTO that drives a 55kW generator using a conventional hydro-static transmission. The transmission allowed operating the generator at fixed speed while at the same time controlling the load force on the buoy. Other types of PTO systems have also been proposed or tested for Wavestars, such as discrete displacement hydraulic cylinder with high pressure accumulators and magnetic lead screws driving conventional generators. According to the Wavestar experiences, it was stated in [37] that the success of wave energy was largely dependent on advancement in PTO technology, thus it might be also of critical importance for wind and wave hybrid power generation platform.

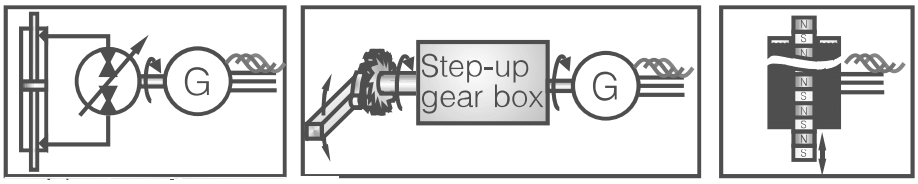

Figure 10: PTO systems for oscillating body WECs [35].

Same as Wavestar model, hydraulic PTO is used in the WECs of DWC concept as illustrated in Fig. 11. Then, the absorbed power can be quantified as $P_{\mathrm{WEC}} = \tau_{\mathrm{PTO}}\omega_{\mathrm{arm}}$, where ω_{arm} is the rotation velocity of the WEC arm. With the WEC geometry design, arm kinematics in terms of arm length L_{arm} and relative rotational angle θ_{rel} is illustrated in Fig. 12. In order to abstract as much wave energy as possible, the PTO applied load torque τ_{PTO} should be controlled as a function of wave and body movement to keep the buoy in resonant motion in waves.

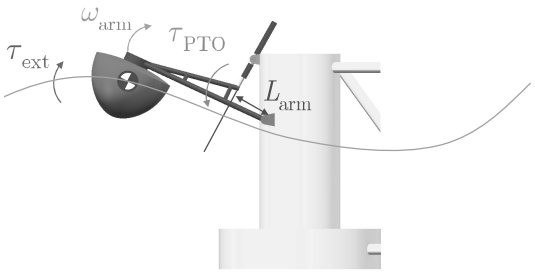

Figure 11: PTO system for DWC WECs.

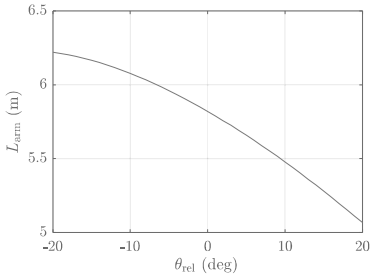

Figure 12: Arm kinematics of the PTO torque.

Different feedback control strategies have been proposed for point-absorber WECs, such as linear damping, reactive control, latching control [37], model predictive control [53]. In this work, three benchmark control schemes, i.e. linear damping (LD), reactive (R) and spring-damping (SD), are chosen to evaluate the PTO control influence on the dyanmic response and power production of the hybrid DWC platform. Specifically, linear damping only allows the response to be attenuated without moving the WEC resonance frequency to the wave peak, while reactive control will inject extra control power in order to absorb a much greater amount of wave energy, which usually acts like a negative spring. Following are the detailed forms of these three PTO control methods, where B_{PTO} is the PTO damping coefficient, K_{PTO} is the virtual spring term in reactive and spring-damping control, ω_{arm} is the rotation velocity and θ_{arm} is the rotation angle of the WEC arm along the shaft of the hinge structure. Then the PTO control torque of the linear damping tau_{LD}, reactive tau_{R} and spring-damping tau_{SD} methods can be respectively expressed as

$$\begin{aligned} \tau_{\mathrm{LD}} &= B_{\mathrm{PTO}}\omega_{\mathrm{arm}} \\ \tau_{\mathrm{R/SD}} &= B_{\mathrm{PTO}}\omega_{\mathrm{arm}} + K_{\mathrm{PTO}}\theta_{arm} \end{aligned} \tag{10}$$

According to [37], optimal B_{PTO} and K_{PTO} can be calculated by

$$K_{\mathrm{PTO}} = \left(J_{\mathrm{WEC}} + J_{\mathrm{add}}\right)\omega^2 - k_{\mathrm{res}} \tag{11}$$

$$B_{\mathrm{PTO}} = B_{\mathrm{hyd}} \tag{12}$$

where J_{WEC} is the inertia of the WEC relative to the shaft, J_{add} is the added inertia of the WEC relative to the shaft, k_{res} is the hydrostatic restoring stiffness coefficient and B_{hyd} is the hydrodynamic damping coefficient. Therefore, the optimal control parameters are calculated to be B_{PTO}= 6.10 MNm/(°/s) and K_{PTO}= -4.34 MNm/°, which are then seen as benchmark linear damping and reactive control parameters. In addition, a positive K_{PTO}= 4.34 MNm/° is used in spring-damping control as another reference case. Dynamic response and power output for DeepCwind and DWC with no PTO control are also obtained for comparative study. Besides, a maximum PTO torque of $\tau_{\mathrm{PTO,max}} = 5$ MNm is applied in all the numerical simulations. Note that all the control strategies are implemented in a user-defined DLL called by AQWA.

3.5. Mooring system

For mooring system dynamic analysis in AQWA, The lumped-mass approach is applied to establish the dynamic composite catenary mooring line model consisting of multi-segment elastic catenary lines. Each catenary segment is specified by length, mass, equivalent cross-sectional area, axial stiffness, drag forces, inline elastic tension and bending moment properties. The interaction between the platform and the mooring lines is fully coupled. The sea bed is modelled with nonlinear springs and dampers in order to minimize energy losses and discontinuities due to the discretization. Details of the mooring line equations are not presented here for brevity, which can be found in [47].

3.6. Model Verification

In order to ensure the modelling correctness, particularly for the coupled aero-hydro-servo-mooring behaviours of DeepCwind FOWT, dynamic responses of the established model in AQWA have been used to verify against the FAST results. Regarding Wavestar, potential flow based AQWA is not compared with other WEC dynamic simulation tools such as WEC-Sim [54], since it has already been widely adopted in dynamic analysis of point absorber WECs. Three different environmental conditions are considered in the verification process.

The first scenario is free decay test without aerodynamic loads or incident waves. The initial condition of the semi-submersible platform is set as 5 m surge, 2 m heave and 5° pitch. As shown in Fig. 13, the platform surge, heave, pitch and fairlead tension dynamic responses agree very well with each other, demonstrating the load calculations with regards to hydrostatics, gravitations, moorings, and part of hydrodynamics (i.e. added mass, radiation damping and viscous drag) are credible.

Second environmental condition includes 11.3 m/s steady wind and regular wave with 1.5 m H_s and 10 s T_p, so that aerodynamic loads (rotor thrust and torque) can be evaluated, and hydrodynamic

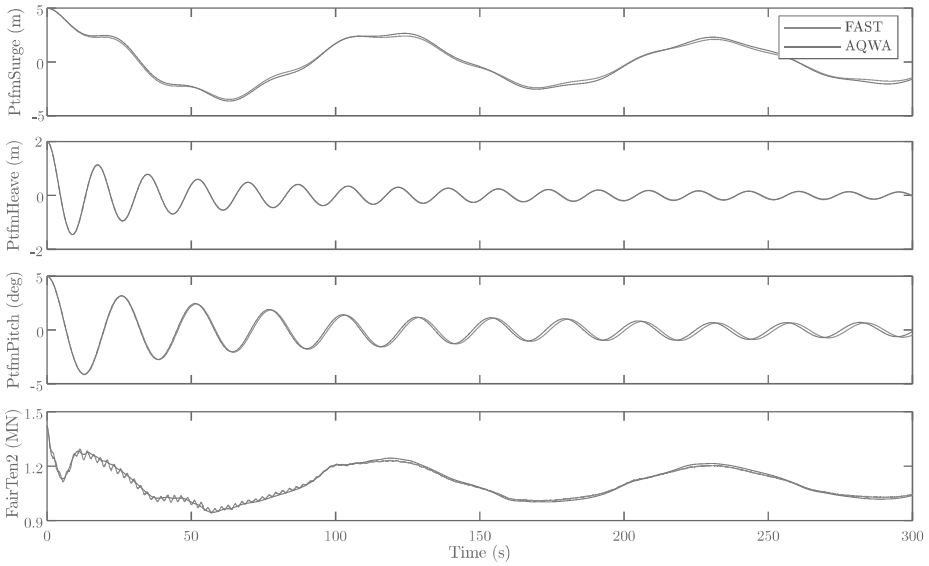

Figure 13: Free decay result comparison between FAST and AQWA (No aerodynamic or incident wave loads).

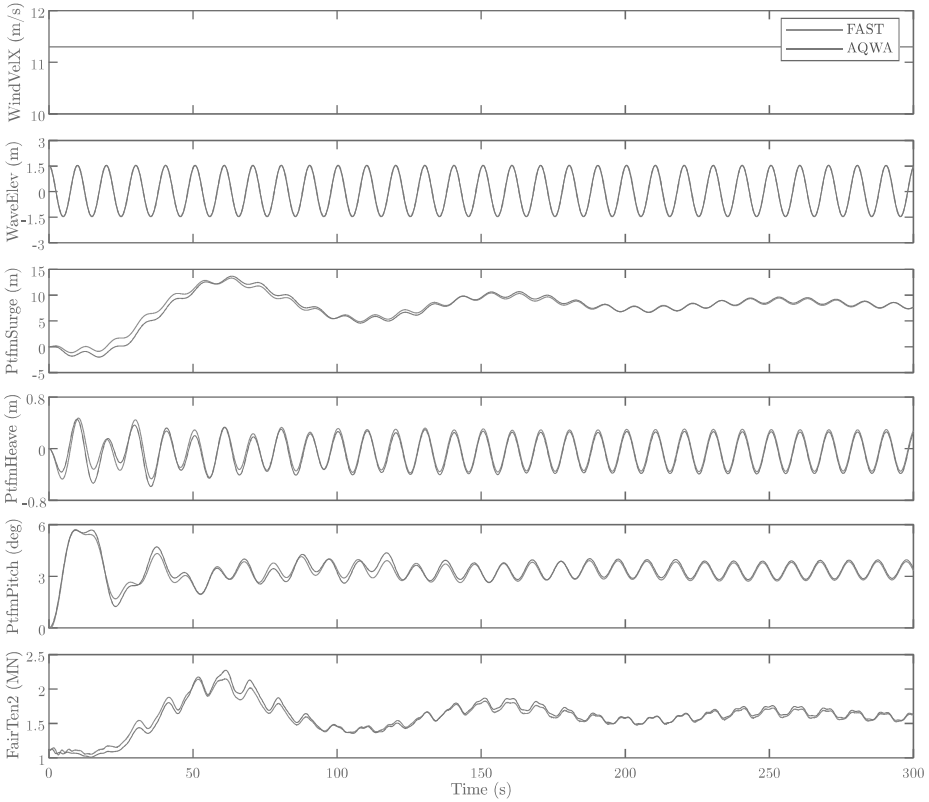

Figure 14: Dynamic response comparison between FAST and AQWA (11.3 m/s steady wind, regular wave with 1.5 m H_s and 10 s T_p).

loads (incident waves, added mass, radiation damping and viscous) can be further verified as well. The 11.3 m/s wind speed is chosen as it generates the highest aerodynamic loads. Besides, additional simulations with 30°, 60° and 90° wind-wave misalignment have been conducted. It can be observed from Fig. 14 and 15 that the obtained dynamic responses from AQWA, including sway and roll, still show good agreement with the FAST results even with wind-wave misalignment. However, the environmental condition is close to steady-state, while large transient dynamic behaviour still needs further verification.

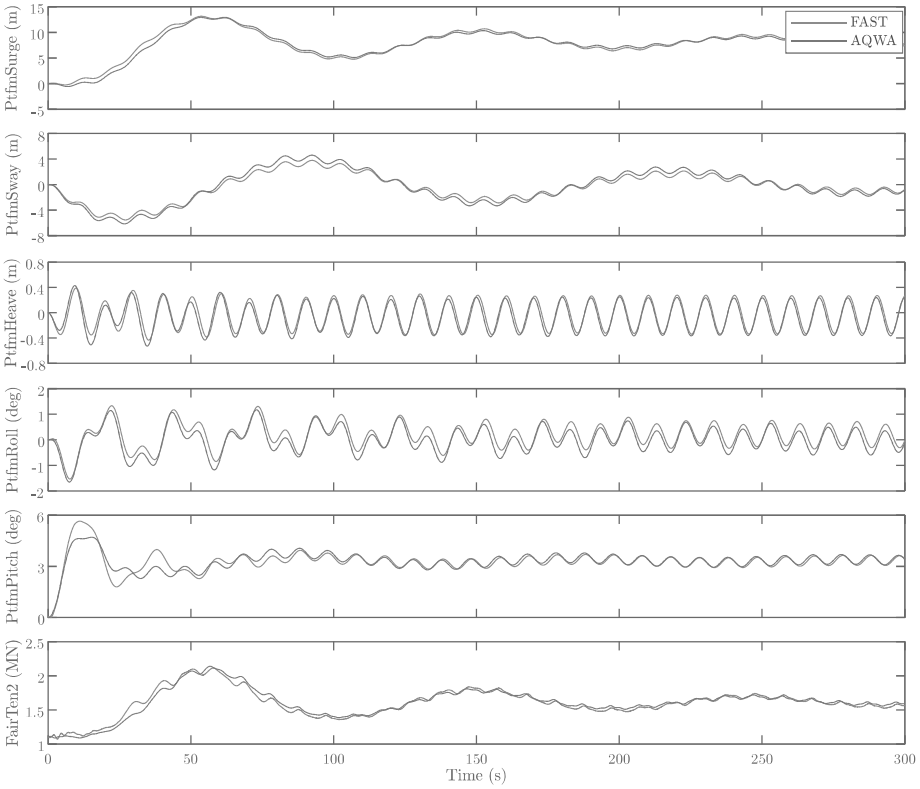

Figure 15: Dynamic response comparison between FAST and AQWA with 60° wind-wave misalignment (11.3 m/s steady wind, regular wave with 1.5 m H_s and 10 s T_p).

The third verification test uses 8 m/s turbulent wind with 15 % turbulence intensity I and irregular wave with 2.5 m H_s and 9.8 s T_p, which is consistent with the environmental condition of the design load cases (DLC) in later DWC dynamic analysis. Fully coupled aero-hydro-servo-mooring dynamics with transient behaviours can be evaluated. As shown in Fig. 16, AQWA and FAST still have good match, but there also exist observable discrepancies, particularly for the surge and pitch motion. This is mainly due to that the aerodynamic load calculation within the established framework is based on steady-state approximation, so that large transient deviation from the equilibrium state could not be perfectly described. Still, in general the established model is able to estimate the motion dynamics of the DeepCwind FOWT with a high level of confidence.

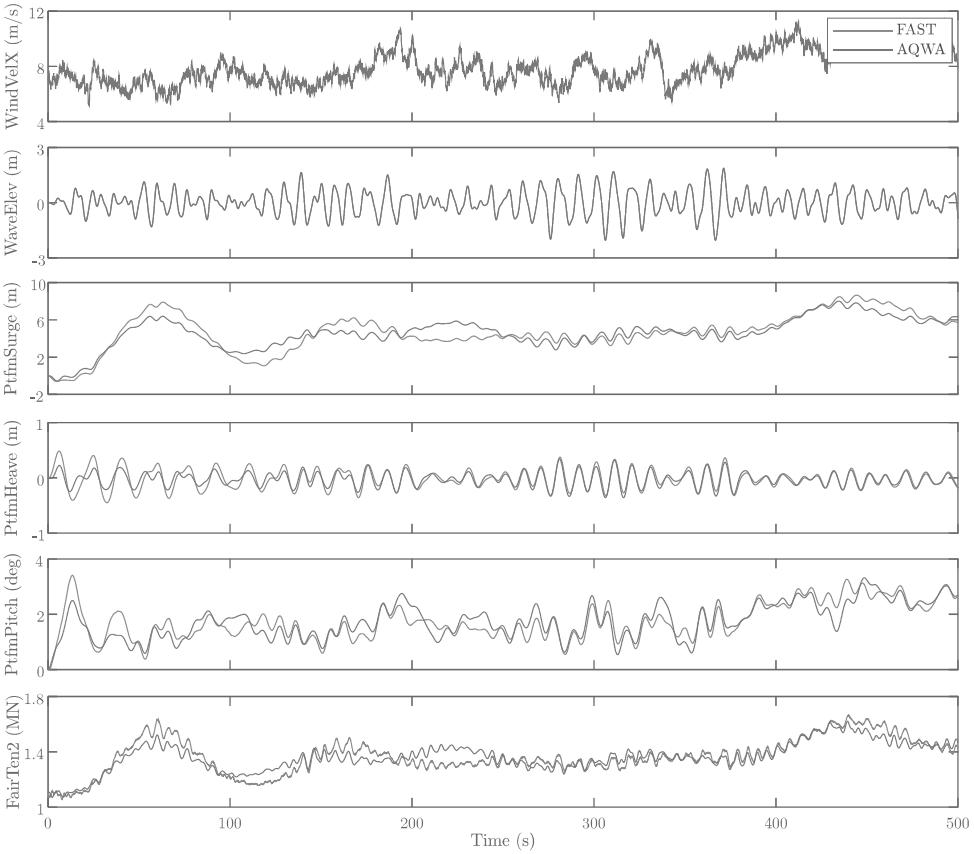

Figure 16: Dynamic response comparison between FAST and AQWA (8 m/s turbulent wind, irregular wave with 2.5 m H_s and 9.8 s T_p).

4. Numerical Simulation and Result Analysis

This section presents the numerical simulation results and analysis for the proposed DWC concept based on the established aero-hydro-servo-mooring framework. Simulation setup within AQWA as well as the chosen environmental conditions for dynamic response analysis and power output evaluation are introduced. Free decay test is firstly performed to investigate the influences of introducing WECs and PTO control on the natural periods of the DWC platform. Then, four typical design load cases (DLCs) with turbulent winds and irregular waves are chosen to study the operational behaviours of the hybrid platform. Note that these DLCs manage to cover different operational regions below the cut-out wind speed in the power curve shown in Fig. 5. Particularly, different PTO control strategies for the three installed WECs as described above are applied in the simulations, and their influences on platform dynamics, mooring loads, and power output are comparatively evaluated.

4.1. Simulation Setup

With the dimensional and structural properties in Table 1-2, the DWC model was built within ANSYS AQWA Workbench environment as shown in Fig. 17, and the generated mesh has been shown above in Fig. 9 with 34997 nodes of 0.96 m maximum element size. The DWC platform is supposed to be moored in an water area of 1800 m × 1500 m with 200 m depth, and the WECs are attached to the DeepCwind offset columns with non-frictional hinge joints. The WEC PTO system is implemented with a user-defined DLL to characterize the control torques as depicted in Fig. 10. The aerodynamic loads are also calculated with a user-defined DLL as described above. Then, hydrodynamic radiation and diffraction analysis for this multi-body system can be performed, so that the frequency-domain parameters and time-domain responses for different DLCs will be obtained.

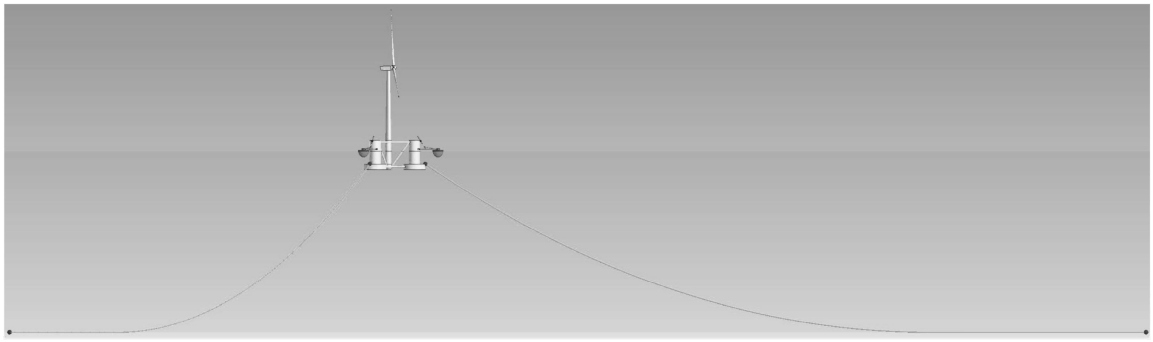

Figure 17: The DWC hybrid model built within ANSYS AQWA Workbench environment.

Four environmental conditions as listed in Table 3 are used in the time-domain simulations. These DLCs are chosen to cover different operational regions in the power curve, including below rated (Region 2), rated (Region 2-1/2), above rated (Region 3), as well as severe sea state in above rated condition (Region 3) with parked WECs. Correspondingly, four mean wind speeds (v), i.e. 8, 11.3, 14, 20 m/s, are used in these simulations, and the turbulent wind time sequence are generated by TurbSim [55] from NREL, where the IEC Kaimal turbulence model and the turbulence intensity (I) of 15%, 15%, 15%, 10% are used for each wind speed. Regarding wave conditions, JONSWAP spectrum is used, and the significant wave height (H_s) and peak period (T_p) can be estimated with the correlation in Equation (4). Besides, for each DLC, six different random seeds are used to generate the turbulent wind and irregular wave time-series to avoid random behaviours. Also, since potential flow solution does not account viscous effect, extra damping is needed to better characterize its dynamic behaviours in real sea states. Fig. 18 illustrates application regions of wave-force formulas for offshore structures [56], and it can be seen that the semi-submersible platform and point-absorber WEC under these DLCs are mostly falling into the small drag region with large inertia. This means the viscous drag is not significant but still cannot be ignored. As indicated by [41], additional quadratic drag needs to be added on top of the potential-flow contribution as implemented with Equation (7). Similarly,

viscous damping with a coefficient C_d of 0.25 is applied to the three WECs, resulting in the quadratic damping coefficients listed in Table 4.

Table 3: Design Load Cases [57, 58].

Category	Case no.	v (m/s)	I (%)	H_s (m)	T_p (s)	WT status	WEC status
WEC Operational	DLC 1	8	15	2.5	9.8	Operational	Operational
	DLC 2	11.3	15	3	10	Operational	Operational
	DLC 3	14	15	3.6	10.2	Operational	Operational
WEC Parked	DLC 4	20	10	4.2	10.5	Operational	Parked

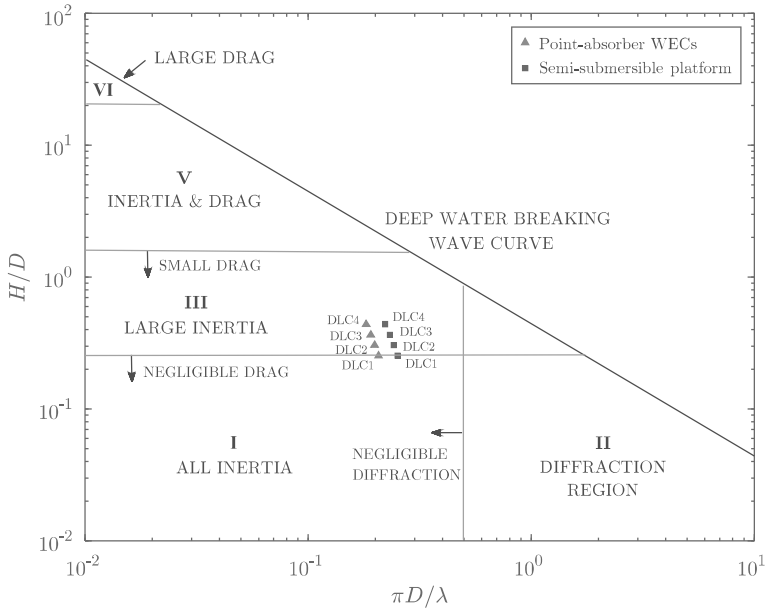

Figure 18: Application regions of wave force formulas for offshore structures.

Table 4: Quadratic drag coefficients C^{ii} for the Semi-submersible platform and point-absorber WECs

	Surge (Ns^2/m^2)	Sway (Ns^2/m^2)	Heave (Ns^2/m^2)	Roll (Nms^2/rad^2)	Pitch (Nms^2/rad^2)	Yaw (Nms^2/rad^2)
Platform	3.95×10^5	3.95×10^5	3.88×10^6	3.70×10^{10}	3.70×10^{10}	4.08×10^9
WEC	4.85×10^3	4.85×10^3	9.76×10^3	2.15×10^4	2.15×10^4	2.17×10^4

As mentioned above, three different PTO control strategies, i.e. linear damping control, reactive control and spring-damping control, are considered in the coupled simulations in order to comparatively study the PTO control influence on the system dynamics and power output performance. Specifically, the optimal damping coefficient B_{PTO} for LD control is to match the radiation damping at the peak wave frequency, which can be calculated by Equation (12). Besides passive linear damping, reactive control introduces an extra spring control torque but in a negative form, which is able to inject

additional energy to excite the buoy motions for resonance. The optimal spring constant K_{PTO} for reactive control can be determined by Equation (11). To better study the spring coefficient influence, a positive spring coefficient with the same absolute value of reactive control is also used, although it will further shift the WEC natural period away from the peak wave period. Besides, DeepCwind floating wind turbine and DWC witout PTO control are seen as two comparison groups. In all, the PTO parameters for these control strategies are presented in Table 5, where the target peak wave period of 10 s is used.

Table 5: Parameters of the applied PTO control strategies.

Parameters	No control	LD control	R control	SD control
B_{PTO} (MNm/(°/s))	0	6.10	6.10	6.10
K_{PTO} (MNm/°)	0	0	-4.34	4.34

For each simulation, the time duration is set as 1000 s with 0.1 s time step, and proper initial position is set in order to eliminate potential startup transient effects for the selected simulation condition. As shown in Fig. 2, all the analysis in this work is within inertial frame and global coordinate system, and the reference point is P. The wind and wave directions are consistent with the positive X direction in the inertial coordinate.

4.2. Free Decay Test

The natural period of the hybrid platform could be altered with the point-absorber WECs installed, so free decay test is performed first to investigate how PTO spring and damping coefficients affect the DWC platform natural frequency. Free decay with different PTO control schemes is also performed. Only longitudinal motions are considered here due to platform symmetry, and the initial surge, heave and pitch conditions are listed in Table 6.

Table 6: Initial condition of free decay simulations.

Test	Surge (m)	Heave (m)	Pitch (deg)
Surge decay	5	0	0
Heave decay	0	2	0
Pitch decay	0	0	5

The variation trends for the natural periods of different motion modes caused by varying K_{PTO} and B_{PTO} are shown in Fig. 19 and 20. It can be observed that the surge natural period is almost not affected by the varying PTO constants, as K_{PTO} and B_{PTO} are not contributing to the surge motion dynamics. In contrast, the heave and pitch natural periods will be shifted with these PTO coefficients. More specifically, regarding K_{PTO}, positive spring load torque will shorten the natural periods of the

hybrid platform, while negative spring coefficients will generally further increase natural periods for heave and pitch modes. This observation also meets our expectation from first principles. However, as not expected, the pitch natural period does not continue to increase when the K_{PTO} reaches -4×10^6 Nm/°. Regarding B_{PTO}, the natural periods for heave and pitch motion will be reduced with increased damping coefficients, and at the same time the platform heave and pitch motions are also noticeably damped with large B_{PTO}.

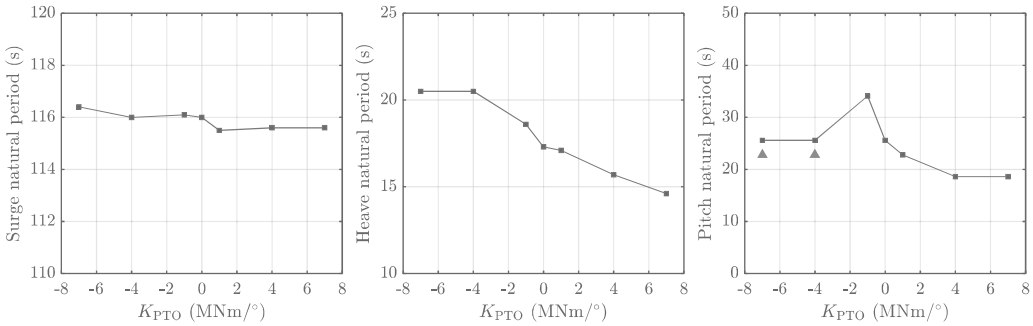

Figure 19: Comparison of natural frequencies of the DWC platform with differnet K_{PTO} coefficients.

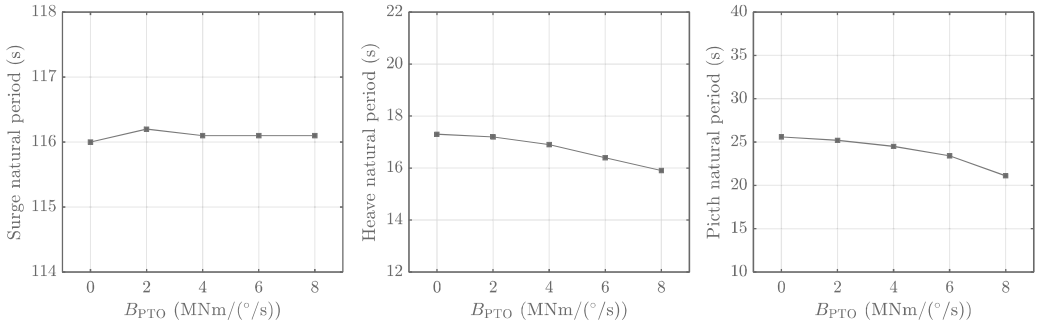

Figure 20: Comparison of natural frequencies of the DWC platform with differnet B_{PTO} coefficients.

Free decay simulations with four selected PTO schemes in Table 5 are also performed to investigate the PTO control influence on the hybrid platform natural periods. Motion responses and statistical results are presented in Fig. 21. It can be noticed that the surge natural period of the DWC platform is larger than that of DeepCwind. This is due to the increased surge mode added mass from the three point-absorber WECs. For different PTO control strategies, the surge natural frequency keeps almost the same, which is consistent with the above analysis. Regarding the heave motion of DWC platform, its natural period is shorter than that of DeepCwind, which is mainly due to the increased hydrostatic stiffness resulting from the three installed WECs. Moreover, with the introduction of PTO damping terms, the heave natural period is further shortened as it will contribute to larger equivalent hydrostatic stiffness. For PTO spring terms, the negative coefficients in reactive control will help increase the heave natural period while provides more heave damping at the same time, and vice versa

for spring-damping control. Pitch natural period is similarly affected as heave. Besides, also notice the large negative spring PTO torque in reactive control will provide a large overturning moment, so that the DWC platform cannot return to the zero equilibrium state.

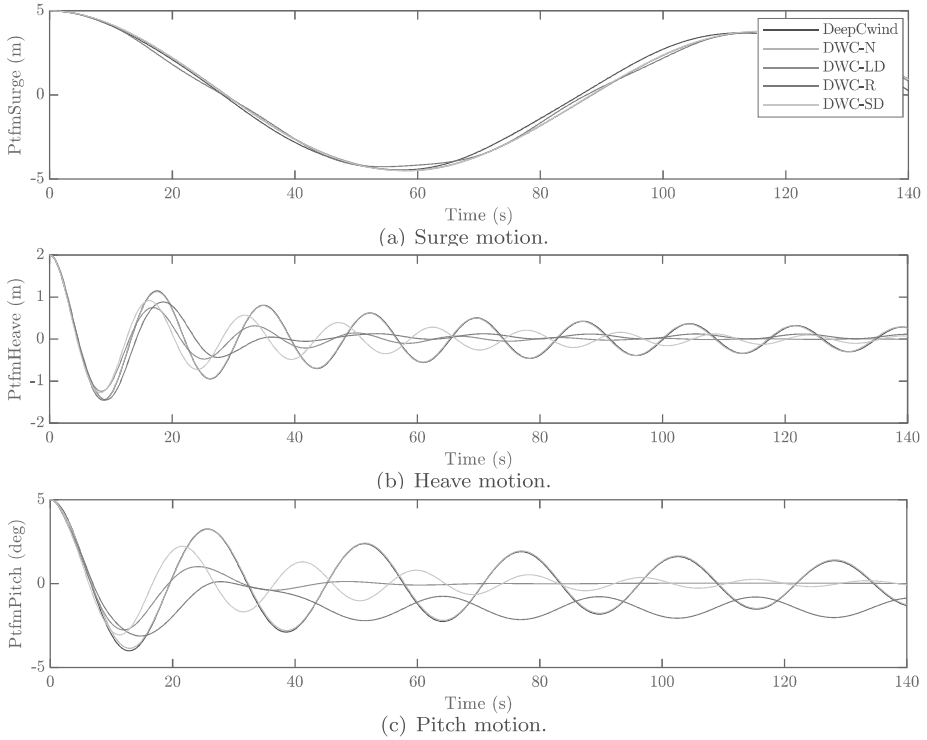

(a) Surge motion.

(b) Heave motion.

(c) Pitch motion.

Figure 21: Free decay motion responses with different PTO control strategies.

Table 7: Comparison of natural periods with different PTO control strategies.

	DeepCwind	DWC-N	DWC-LD	DWC-R	DWC-SD
Surge (s)	113.5	117.0	117.0	117.0	117.0
Heave (s)	17.5	17.2	16.6	17.4	15.3
Pitch (s)	25.8	25.6	24.2	25.6	18.8

4.3. Test with Operational WECs

In this subsection, numerical simulation results for the DLCs with operational WECs are presented, i.e. DLC 1-3 as marked in Fig. 5. The dynamic responses, mooring tensions and power production of the proposed DWC hybrid platform with different PTO control strategies are evaluated.

4.3.1. Platform Motion Comparison

Time series and power spectrum of the DWC platform surge, have and pitch motion responses with operational WECs for DLC 1-3 are shown in Fig. 22-27. The motions of sway, roll, and yaw are

not discussed because they are very small due to the symmetry of structures and external loads. In particular, the influences of PTO control strategies on platform motion dynamics are assessed, and the statistical comparison is summarized in Table 8.

It can be noticed from Table 8 that the added WECs with different PTO control have no significant influence on the DWC surge motion, and the mean, standard deviation (STD), as well as max/min displacement variations are mostly within 3%, while the STD for DLC 2 is slightly increased by over 5% except the spring-damping control. This is due to that the surge motion response is mainly dominated by the wind-induced loads, so that the WECs do not create much influence on the surge dynamics, although they will increase the added mass and hydrodynamic damping such and suppress the wave-induced motion response as observed from the surge power spectra.

Regarding heave motion, reactive and spring-damping control schemes are shown to generate higher impacts than linear damping and no control, which indicates the PTO spring terms are closely relevant to platform heave mode. More specifically, mean heave displacement is increased by 177% with reactive control and decreased by 40% for spring damping control, showing an adverse effect brought by these two control designs with opposite spring constants. While the heave STD are both largely increased, and reactive control has even lead to a rise of 30% in DLC 1. This means the spring terms in PTO control will intensify the platform heave motion response. In contrast, linear damping and no PTO control produce less heave dynamics variations of below 3%. PSD curves indicate the heave motion is dominated by the wave-induced response and its own resonance. It shows again that reactive and spring-damping control will increase the heave resonant response, leading to more intensive heave motions. Linear damping also intensities heave resonance to certain extent, but it is also mitigating the wave-induced response, so that the heave STD is reduced by around 3%.

Platform pitch motion is of more importance as it is closely relevant to the ultimate and fatigue loads of critical wind turbine structures, such as tower and blades. It can be observed from Table 8 that the pitch response is not much affected by the added WECs with no PTO control. If linear damping applied, the STD of pitch motion will be increased by over 10% for DLC 2-3, while its influence on mean pitch is negligible. In contrast, reactive and spring-damping control will have significant influence on DWC pitch dynamics. For Reactive control, the mean pitch angle is increased by 47-63%, and 27-39% for pitch STD. The severe negative impacts on pitch are harmful to the structural life of the supported wind turbine, as well as the stability of power output. On the contrary, spring-damping PTO control reduces the mean pitch by 23-29%, and the STD could be decreased by 23% for DLC 1 though not much improvement for DLC 2-3. PSD curves indicate the pitch responses are mainly affected by wind-induced motion, pitch resonance and wave-induced motion. Linear damping PTO control causes aggravate wave frequency response, so that pitch STD is increased by over 10% for DLC 2and 3, which corresponds to the statistical results. For reactive control, it is deteriorating all the wind and wave frequency responses and the pitch resonance, especially the low-frequency wind

induced motion is highly increased, which results in more vigorous pitch for DWC. On the contrary, spring-damping control is noticeably suppressing wind-induced and pitch resonance responses, leading to mitigated DWC pitch motion.

Apparently, the WEC PTO control schemes are shown to have significant impacts on the platform motion dynamics of the proposed floating wind-wave hybrid platform. More specifically, reactive control generally introduces negative influence on the platform motion responses, while spring-damping control is able to mitigate the pitch motion to certain extent. DWC with linear damping, which is used by most previous works [24], are prone to much less significant influence on dynamic responses. Also note that the PTO control strategies used in this work are mainly designed for obtaining more wave power, while not much consideration is laid on platform motion mitigation. Therefore, the discrepant results indicate that better platform dynamics performance could be achieved with proper PTO control design, for instance OCIR control proposed in [37], which is to be further investigated in our further works.

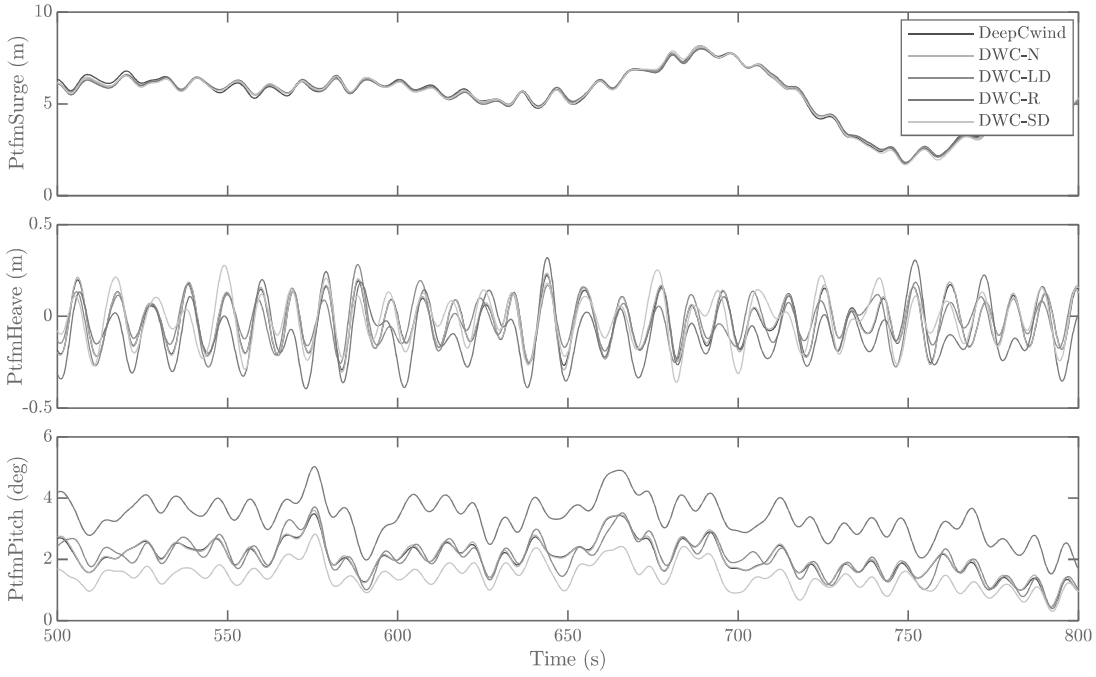

Figure 22: Platform motion response time-series in DLC 1.

4.3.2. Mooring Tension Comparison

Mooring tensions of the DWC concept with different PTO control strategies have also been investigated. Mooring line 2 is chosen here as it is supposed to suffer the most severe dynamic loads, and the tension load response time-series are shown in Fig. 28, and the statistical results are presented in Table 9. Since mooring tension is mainly coupled with the surge dynamics of the floating platform, the

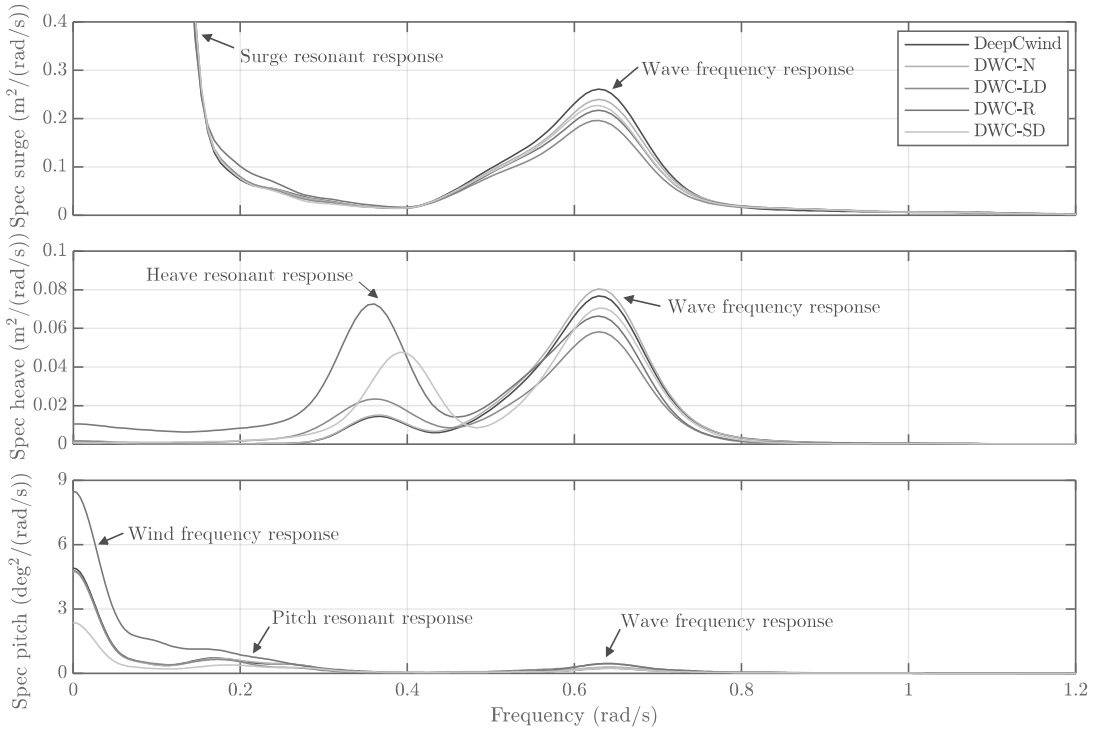

Figure 23: Smoothed power spectra of platform motion response in DLC 1.

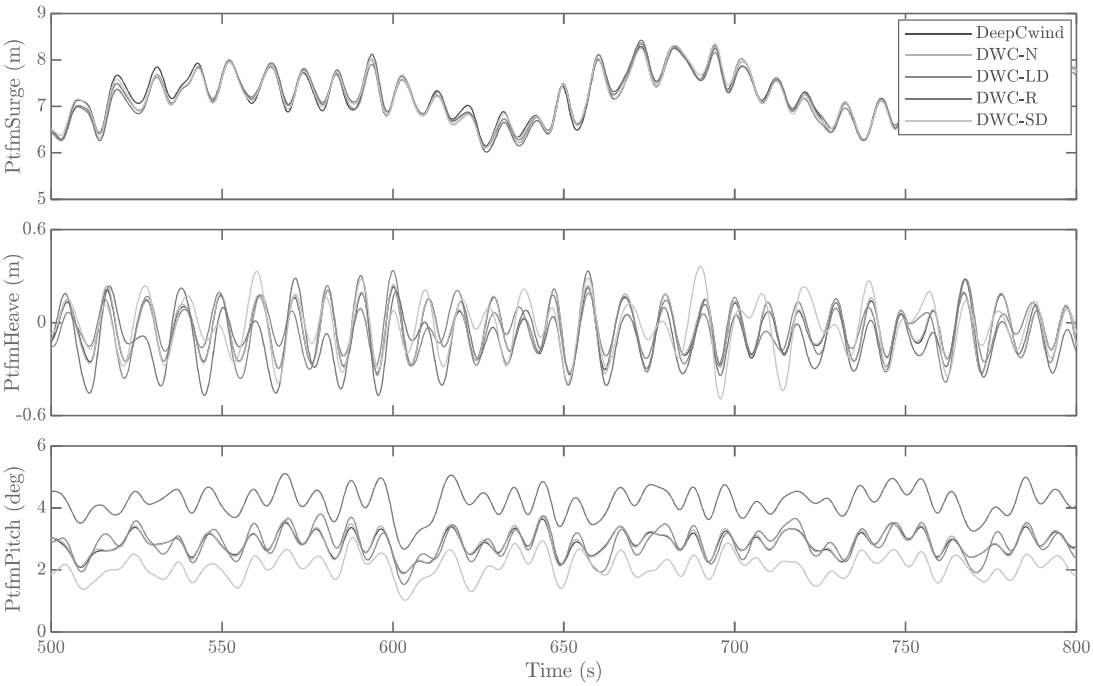

Figure 24: Platform motion response time-series in DLC 2.

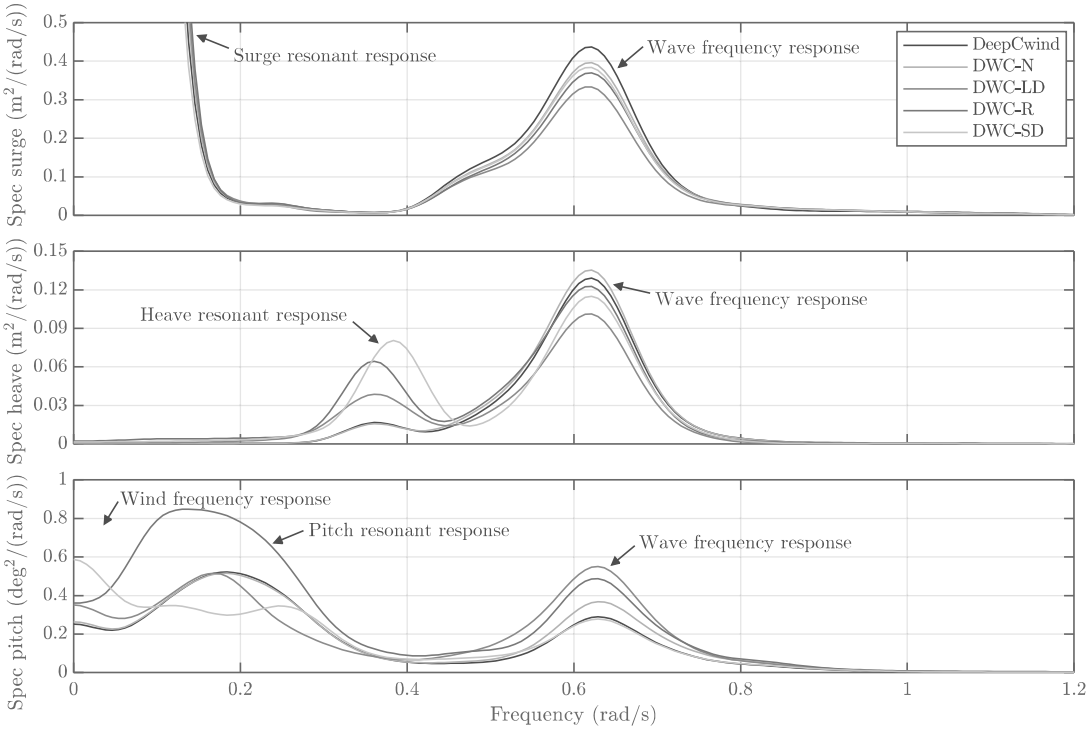

Figure 25: Smoothed power spectra of platform motion response in DLC 2.

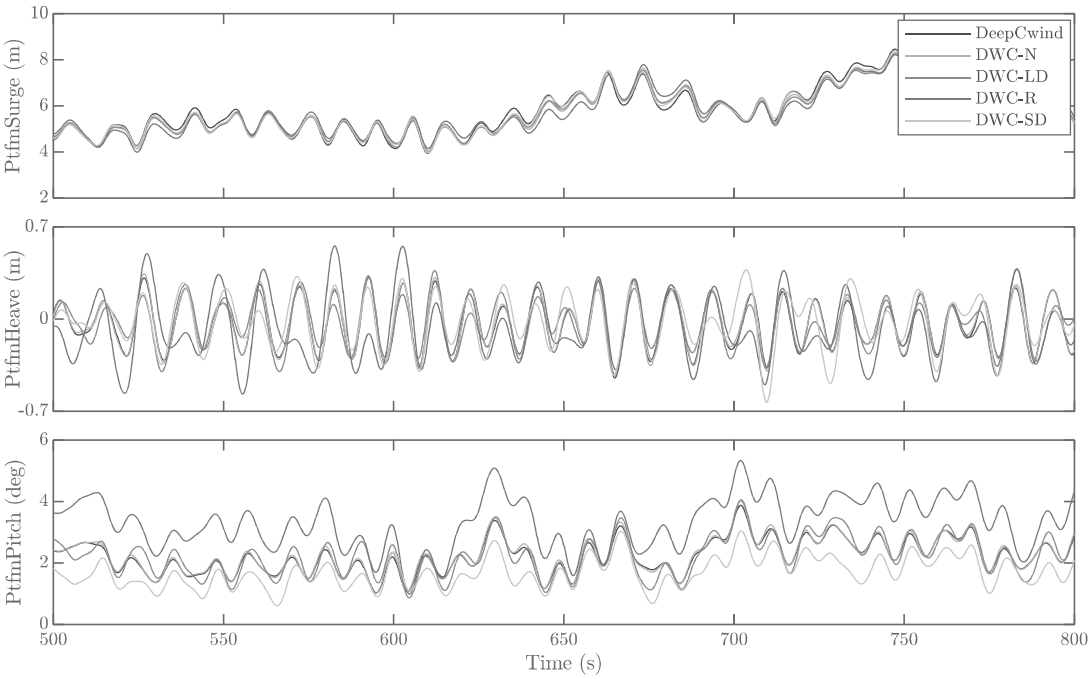

Figure 26: Platform motion response time-series in DLC 3.

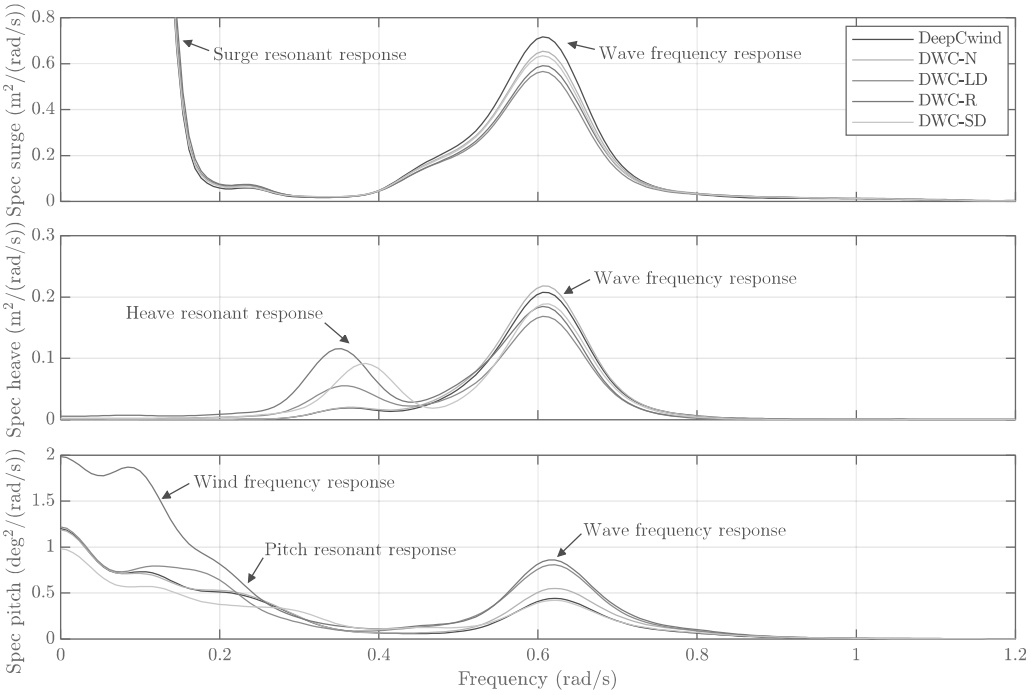

Figure 27: Smoothed power spectra of platform motion response in DLC 3.

Table 8: Platform motion comparison of DWC relative to DeepCwind. (+ Percentage increase, - Percentage decrease)

DLC	Parameters	DWC-N			DWC-LD			DWC-R			DWC-SD		
		Surge	Heave	Pitch	Surge	Heave	Pitch	Surge	Heave	Pitch	Surge	Heave	Pitch
DLC 1	Mean	-0.11	-7.76	1.13	-0.29	1.93	1.02	-0.24	**177.10**	**63.07**	-0.19	**-40.38**	**-29.98**
	Std	0.47	2.91	0.12	-0.31	-2.67	2.87	0.71	**30.29**	**39.82**	1.67	**10.09**	**-23.81**
	Max	-0.84	5.98	3.17	-2.07	-5.35	6.47	-1.83	19.93	44.18	0.02	-1.54	-19.10
	Min	1.94	2.59	2.86	3.90	5.33	-11.92	2.81	18.83	-43.47	-3.08	21.34	-108.68
DLC 2	Mean	-0.19	-7.13	0.54	-0.36	0.12	0.35	-0.14	**118.00**	**46.96**	-0.17	**-39.21**	**-26.97**
	Std	6.76	2.77	5.01	5.64	-1.46	**12.48**	5.87	**14.21**	**26.86**	1.12	**9.37**	**6.59**
	Max	3.52	5.10	5.35	4.11	-4.93	9.12	2.51	15.22	38.10	2.13	2.19	-10.39
	Min	1.21	1.49	-2.60	-0.05	3.65	1.73	0.56	-4.06	63.60	1.42	12.95	-40.77
DLC 3	Mean	-0.44	-13.84	1.50	-0.71	-0.43	1.39	-0.59	**86.42**	**48.88**	-0.46	**-32.10**	**-23.44**
	Std	2.60	3.03	3.58	3.37	-2.19	**13.27**	3.46	**15.79**	**38.60**	2.89	**6.03**	**-2.23**
	Max	-0.49	6.28	3.62	-0.30	-7.73	4.68	-0.47	16.44	37.67	-0.22	-1.29	-19.72
	Min	2.31	0.36	-1.68	2.31	1.13	-17.98	5.54	-4.22	-3.92	-2.13	7.60	-65.67

tension load comparison with different PTO control schemes shows similar trends with surge motion. In result, the added WECs with different PTO control also produce insignificant influence on mooring tensions, and the mean, STD, as well as max/min displacement variations are mostly within 3%, while the STD for DLC 2 is slightly increased by over 6% with no PTO control.

425 *4.3.3. Power Production Comparison*

Same as Wavestars, hydraulic PTO for WECs is assumed to be used in DWC concept, and an 80% efficiency for the hydraulic PTO is adopted according to [37]. Power production statistics for both the 5 MW wind turbine and three point-absorber WECs are summarized in Table 10. The absorbed wave energy production time-series with different PTO control schemes are shown in Fig. 29. It is

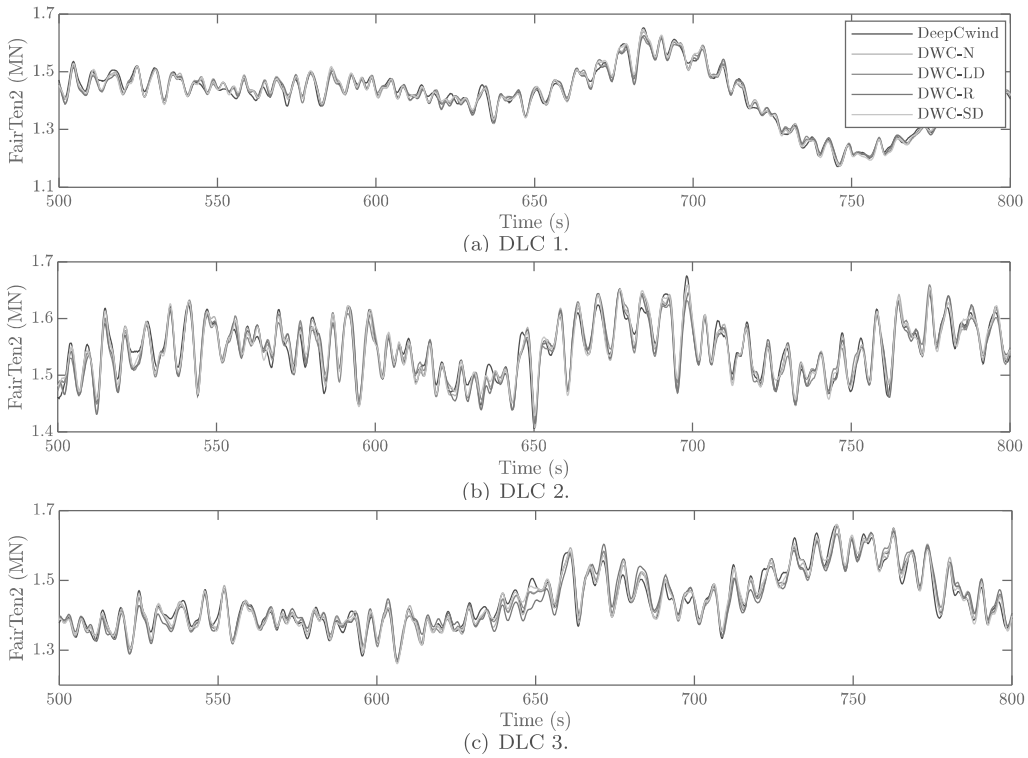

(a) DLC 1.

(b) DLC 2.

(c) DLC 3.

Figure 28: Mooring line 2 tension response time-series.

Table 9: Mooring line 2 tension comparison of DWC relative to DeepCwind. (+ Percentage increase - Percentage decrease)

Case no.	DLC 1				DLC 2				DLC 3			
	Mean	Std	Max	Min	Mean	Std	Max	Min	Mean	Std	Max	Min
DWC-N	-0.02	0.52	-0.86	0.11	-0.06	6.02	0.98	0.32	-0.11	2.74	0.82	0.17
DWC-LD	-0.07	-1.06	-1.79	0.90	-0.11	1.16	1.29	0.76	-0.18	1.67	0.87	0.27
DWC-R	-0.12	-0.50	-1.65	0.27	-0.11	3.25	0.32	0.02	-0.18	2.62	1.52	0.23
DWC-SD	0.01	1.65	-0.35	0.26	0.01	-0.43	0.04	1.09	-0.08	2.10	0.47	-0.42

clearly seen that reactive control leads to the highest wave power generation as expected, followed by linear damping and spring-damping control. More specifically, the absorbed wave energy from reactive control could reach 8.84%, 5.10% and 5.19% of the wind turbine power output for DCL 1-3, respectively. These values for spring-damping control, i.e. 4.54%, 3.04% and 3.10%, are almost the half. This has demonstrated that the PTO control strategy impacts greatly on the WEC power output of the hybrid DWC platform, which needs to be further optimized in future study. Besides, it can be noticed that the absorbed wave energy takes up a bigger portion of the wind-wave power output in below-rated condition than above-rated. This will help produce great supplements for under-rated wind power output, thus largely improving the power quality of the hybrid system. At the same time, these PTO control schemes do not seem to have much influence on wind turbine power generation, the variations of which are within 1% for all DLCs.

Table 10: Mean power production comparison. (MW)

Case no.	DeepCwind	DWC-N		DWC-LD		DWC-R		DWC-SD	
	WT	WECs	WT	WECs	WT	WECs	WT	WECs	WT
DLC 1	2.0475	0.0000	2.0474	0.1358	2.0477	0.1803	2.0404	0.093	2.0502
DLC 2	4.3103	0.0000	4.3103	0.1783	4.3106	0.2196	4.3028	0.1312	4.3132
DLC 3	4.7458	0.0000	4.7458	0.2251	4.7457	0.2464	4.7445	0.1472	4.7465

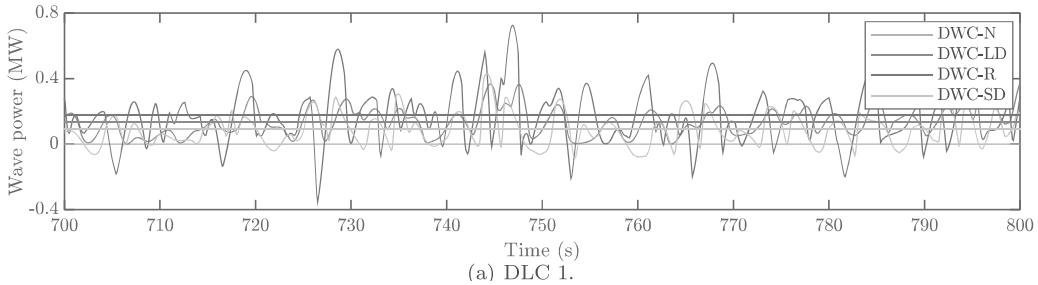

(a) DLC 1.

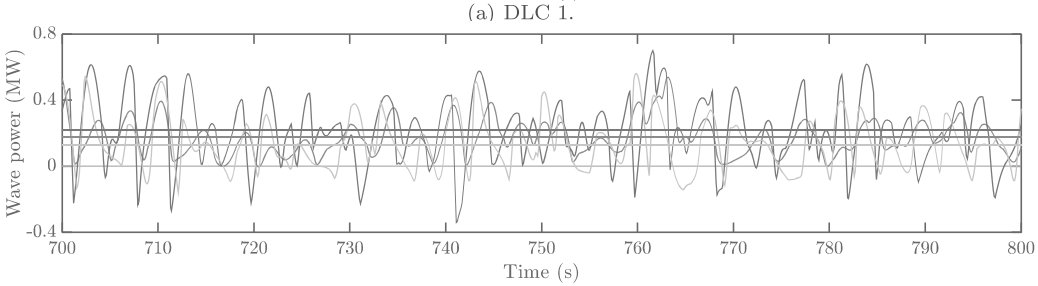

(b) DLC 2.

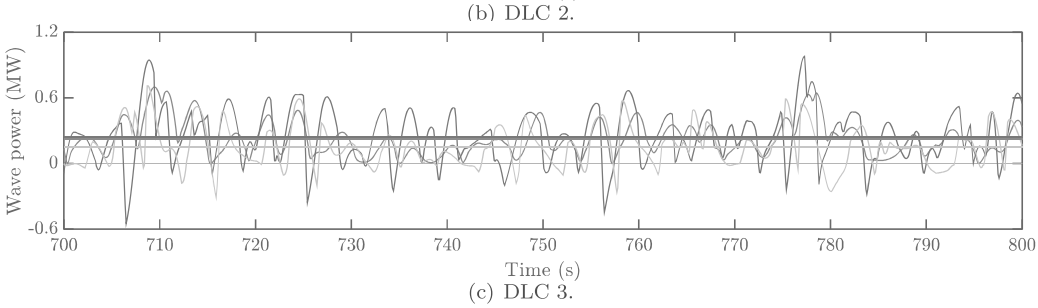

(c) DLC 3.

Figure 29: Wave power production comparisons.

To better study the WEC control behaviour, a small section of the simulations with three different control schemes for WEC 2 in DLC 1 is illustrated in Fig. 31. Time-series of the exciting wave torque τ_{ext}, PTO control torque τ_{PTO} as well as the arm rotation velocity ω_{arm} are plotted. Sea surface elevation and the WEC 2 heave motion are also drawn. It can be clearly seen that reactive control will lead to more rigorous buoy heave motion than the other two PTO control schemes. Meanwhile, the PTO control torque is largely restricted by the saturation threshold, which has prevented the WEC from capturing larger amount of wave power. Therefore, the assumed optimal reactive control design is still not the best solution for WEC power absorption in the floating wind-wave hybrid power generation platform due to the system non-linearities, such as control saturation and floating platform motion. Further investigations have been conducted to indicate the complexity of PTO control influence on

wave power production. Additional numerical simulations under DLC 1 with various K_{PTO} and B_{PTO} are performed, and the smoothed contour map for wave power outputs is shown in Fig. 30, where the results for the selected linear damping, reactive and spring-damping control have been marked. Apparently, the assumed optimal K_{PTO} and B_{PTO} for single DOF point absorbers on fixed structures are not the best solution for the floating WECs in regards to wave power harvesting. Besides, there are more advanced PTO control methods worth investigating, such as model predictive control and oscillation control implemented resistively [59]. In the future, WEC power increment and platform motion mitigation could be both possibly achieved by further studying the WEC buoy number and shape, arm length, as well as more suitable PTO control strategies.

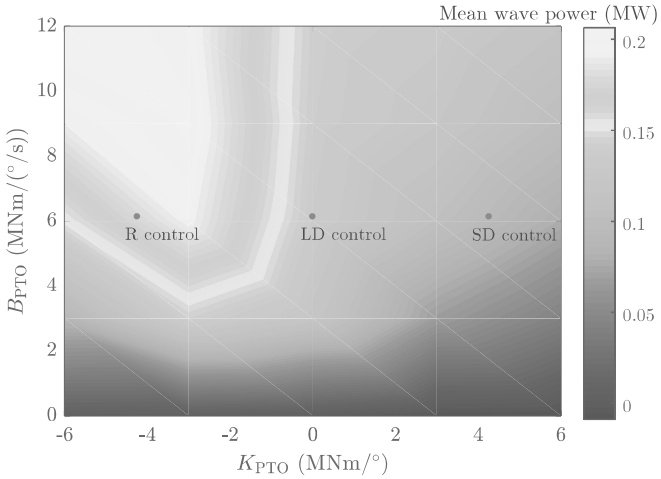

Figure 30: The wave power output smoothed contour map in DLC 1.

4.3.4. PTO Saturation Analysis

It can be seen from Fig. 31 that the PTO control torque is often saturated, in particular for reactive control and spring-damping control. Therefore, further analysis is needed to check whether the above findings are still true without or with saturations of other values. Here, besides 5 MNm, another two PTO saturation torques, i.e. 10 MNm and 15 MNm, are selected, and coupled simulations under DLC 1-3 were conducted again. The platform pitch motion responses and wave power production with different PTO torque saturations under DLC 1 are shown in Fig. 32, and the WEC 2 PTO control torque time-series are illustrated in Fig. 33. Results for the other two DLCs are not attached here for brevity.

Notice from Fig. 33 that the linear damping and spring-damping control torques are not saturated at all with the 15 MNm threshold. At the same time, it can be observed from Fig. 32(a) that the linear damping control influence on mean platform pitch is still small with the other two saturation options, while the spring-damping control is improving the pitch motion with all saturation configurations. In contrast, the reactive control torque keeps saturating even with the 15 MNm threshold, while the

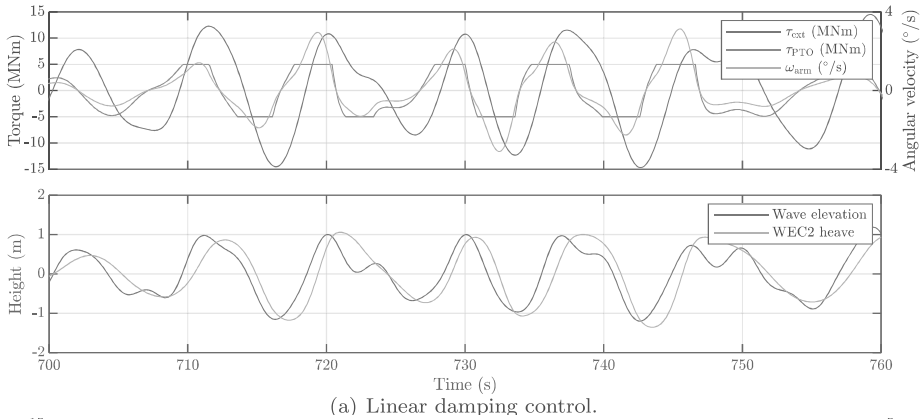

(a) Linear damping control.

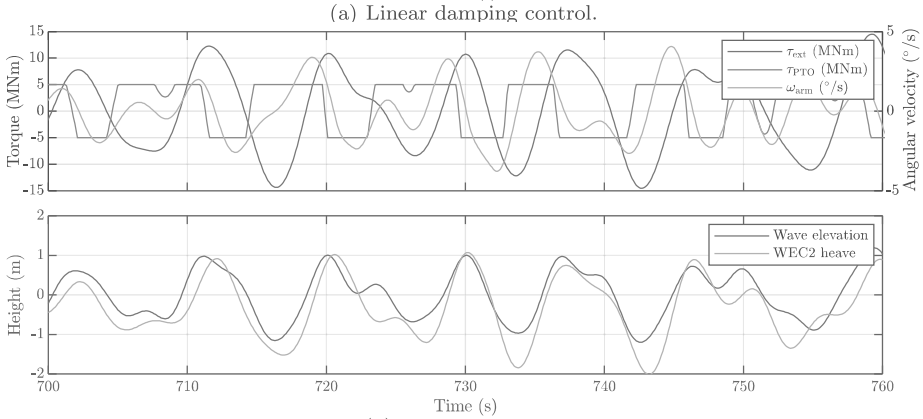

(b) Reactive control.

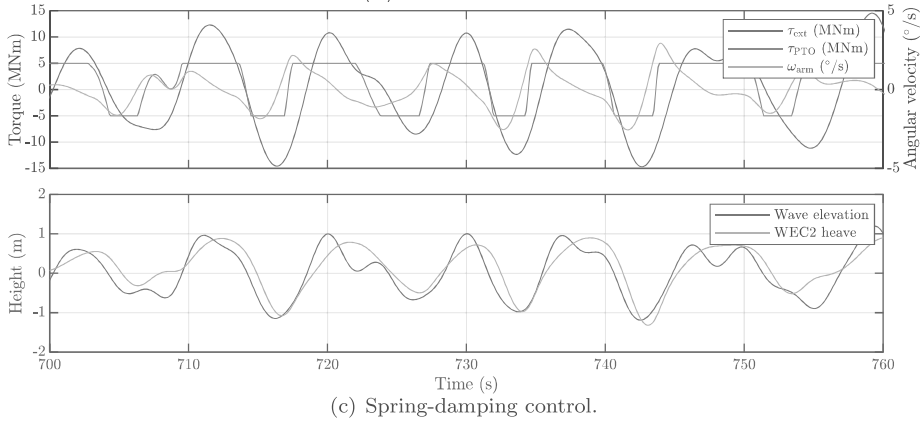

(c) Spring-damping control.

Figure 31: Comparison of PTO control strategies for WEC 2 in DLC 1.

mean platform pitch angle is still in an increasing trend with the growing saturation limits. This has demonstrated that the above remarks about PTO control influence on platform pitch motion responses are still valid with other PTO saturation settings. The WEC power outputs shown in Fig. 32(b) also supports this view, as the reactive control still leads to the highest wave power generation with other saturations. Simulation results for the surge and heave motions as well as mooring loads have similar trends, which is also the same for DLC 2-3. Therefore, the PTO control saturations are not affecting the conclusions drawn above.

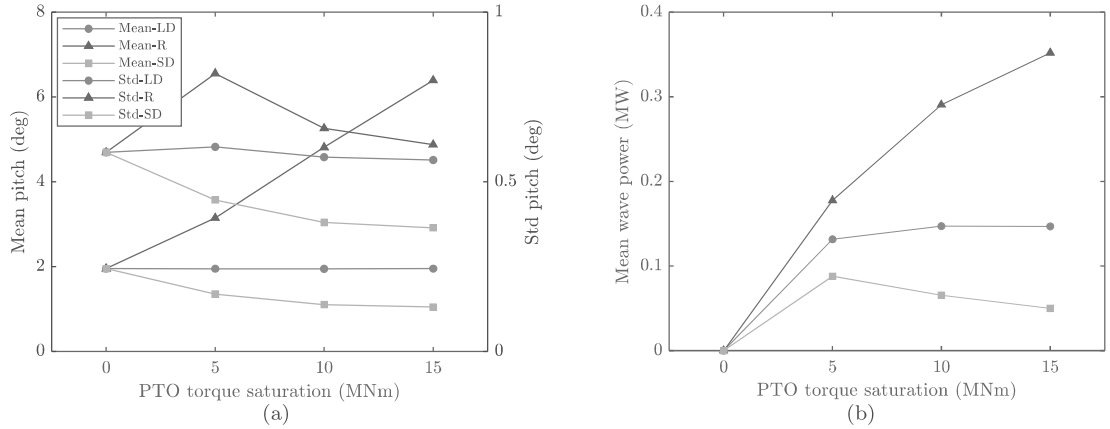

Figure 32: Platform pitch motion responses and wave power production with different PTO torque saturations under DLC 1.

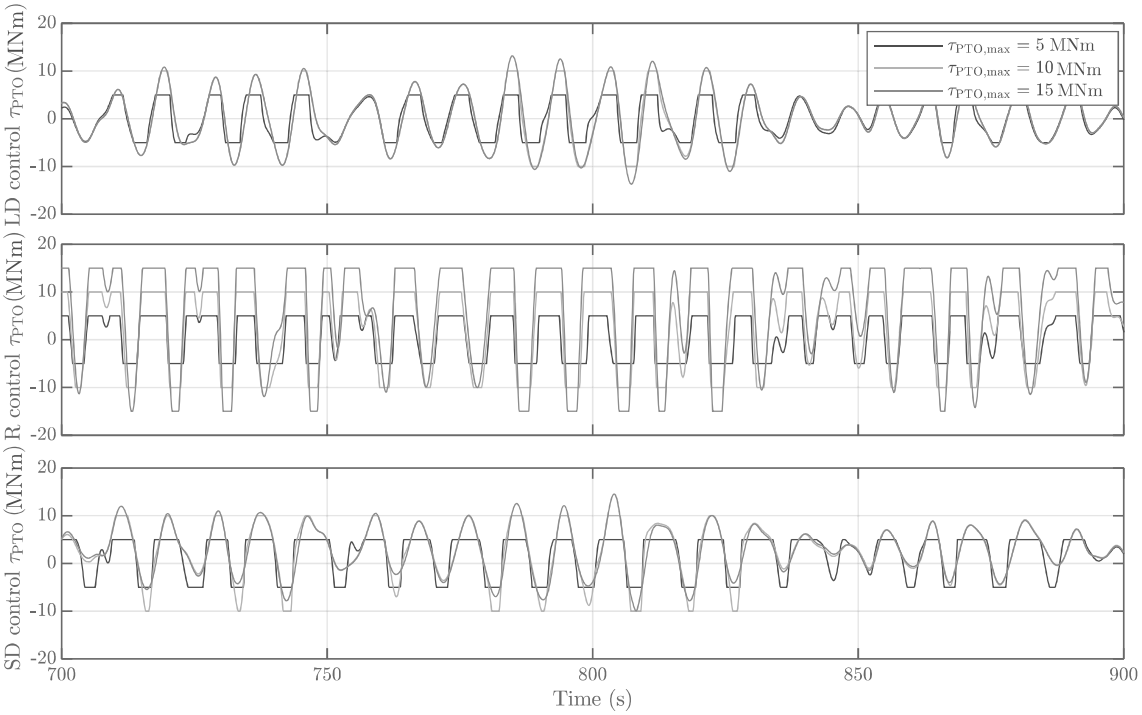

Figure 33: WEC 2 PTO control torque time-series with different PTO torque saturations under DLC 1.

However, it can be noticed from Fig. 32(a) that the mean pitch angle of over 5° resulted from 10 and 15 MNm saturation thresholds has already been a dangerous value for wind turbine structures, indicating the high risks of component failure under huge gravitational loads with large inclination angles. Therefore, the 5 MNm control torque saturation is used in the simulations of this work as a conservative choice, with which it is still feasible to demonstrate the PTO control impacts on motion responses and power production.

4.4. Test with Parked WECs

In Wavestar storm protection mode, water ballast will be pumped out and the buoy will be lifted out of water surface. Similarly, WECs in DWC concept will also be lifted up in rough sea state for protection, such as DLC 4. In default, the ballast water will be all pumped out, leaving the buoy mass of 80000 kg been lifted by the hydraulic cylinder of all three WECs. Alternatively, certain amount of ballast water could be remained inside one buoy, say 140000 kg buoy mass, resulting in a non-symmetrical WEC configuration. This design could be used for counteracting the aerodynamic thrust induced platform imbalance.

Fig. 34-35 and Table 11 present the time-series, power spectrum and the statistical results for the coupled DWC dynamic simulation in DLC 4. Platform surge motion is again not much affected, while the DWC platform draft is increased by 0.6-0.8 m due to the reduced WEC buoyancy. Regarding pitch motion, the mean pitch angle for symmetrical configuration is increased by around 9% (around 0.2°) compared with DeepCwind. This is mainly because of the reduced mooring stiffness caused by the increased platform draft. In contrast, the mean pitch could approach 0° for the non-symmetrical configuration, which is resulting from the WEC weight counter balance, and the pitch standard deviation is also decreased by 0.5%. Note here that the pitch motion reduction will contribute a lot to the ultimate and fatigue load mitigations for wind turbine structures, which is of critical importance to the lifetime of the hybrid power generation platform. Mooring tensions are reduced by 2% in both senarios due to the mitigated platform motion. Similarly, the STDs of wind power output are also reduced by around 2%, meaning potential power output improvement.

Table 11: Comparison of DWC relative to DeepCwind regarding platform motion, mooring tension and power production in DLC 4.

		Surge (m)	Heave (m)	Pitch (deg)	ML2 tension (MN)	Wind power (MW)
DWC (Symm-WECs)	Mean	4.44 (+0.67%)	-0.65 (+1785.17%)	1.70 (+8.89%)	1.33 (-0.73%)	5.00 (0.00%)
	Std	0.68 (-0.58%)	0.27 (-1.06%)	0.41 (-0.21%)	0.05 (-2.38%)	0.04 (-2.00%)
DWC (Asymm-WECs)	Mean	4.42 (+0.16%)	-0.80 (+2210.03%)	-0.01 (-100.83%)	1.33 (-0.89%)	5.00 (0.00%)
	Std	0.69 (-0.38%)	0.26 (-2.86%)	0.41 (-0.52%)	0.05 (1.93%)	0.04 (-2.25%)

5. Conclusions

In this work, we propose a hybrid floating wind and wave power generation platform concept, namely DeepCwind-Wavestar-Combined (DWC), which consists of a well-documented 5 MW semi-submersible FOWT design 'DeepCwind' and three close-to-market point-absorber WEC model 'Wavestars'. Physical parameters and operational configurations have been assumed, resulting in a predicted power curve for the DWC concept. Coupled and verified aero-hydro-servo-mooring numerical simulations are then performed within ANSYS-AQWA environment for different environmental conditions, aiming to preliminarily investigate the concept feasibility in terms of platform motion, mooring line

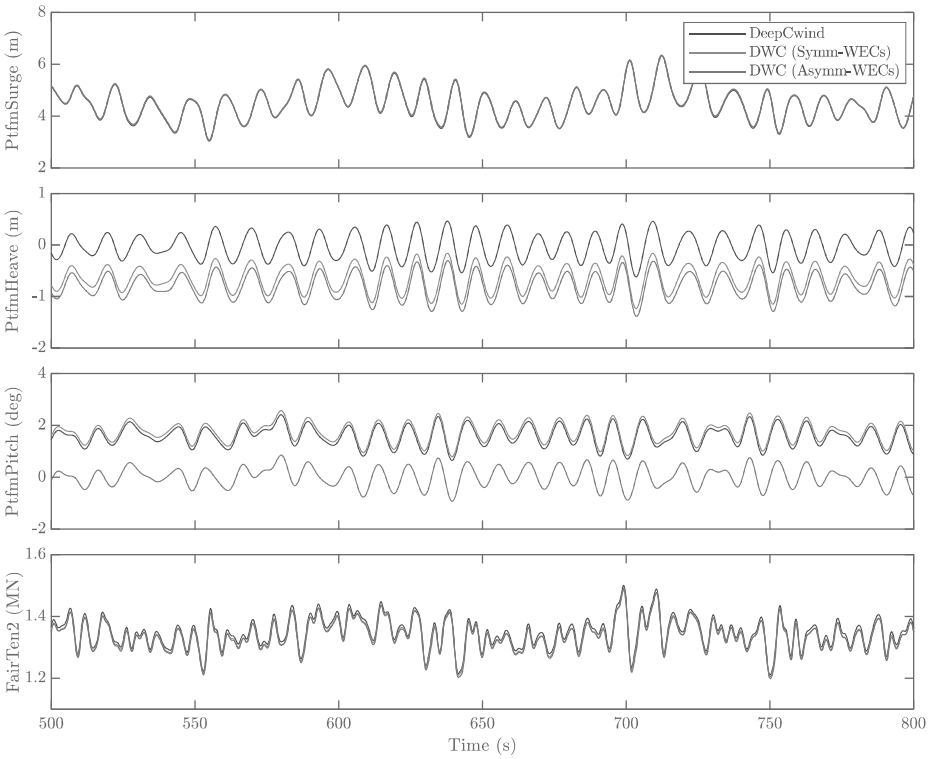

Figure 34: Comparisons of time series of the platform motions, mooring line tension in DLC 4.

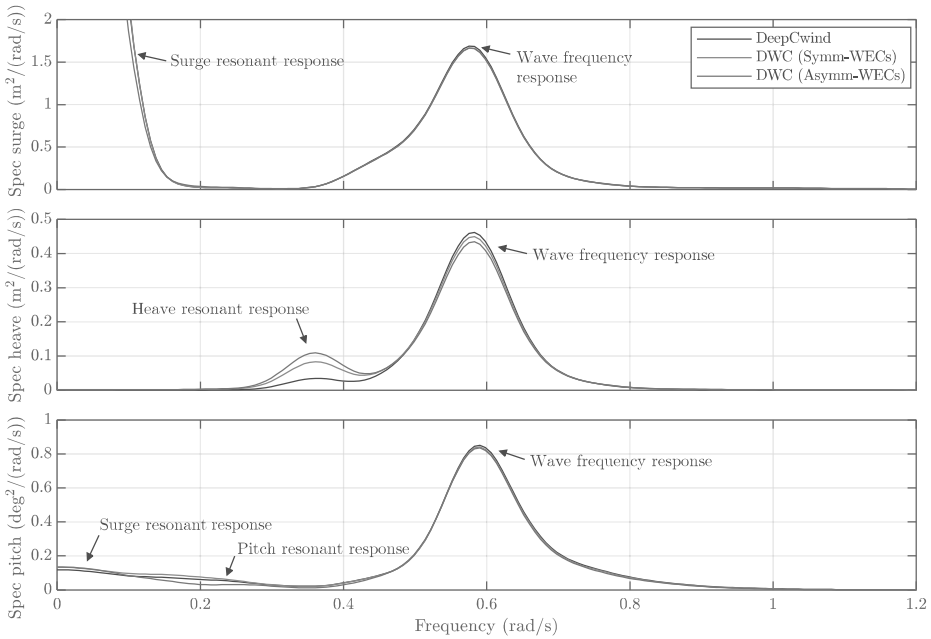

Figure 35: Comparisons of smoothed power spectra of the platform motions in DLC 4.

tension and power production. In particular, different WEC PTO control strategies have been comparatively studied. The following findings can be concluded based on the above numerical simulation result analysis.

1. The surge natural period of the DWC platform is larger than that of DeepCwind, and its surge natural frequency is not much affected by the PTO spring and damping coefficients. In contrast, the heave and pitch natural periods of DWC will be noticeably shifted with varying PTO control constants.
2. The WEC PTO control schemes are shown to have significant impacts on the platform motion dynamics of the proposed floating wind-wave hybrid platform. More specifically, the added WECs with different PTO control show little influence on the DWC surge motion, as it is mainly dominated by the wind-induced loads. Regarding heave motion, reactive control and spring-damping control leads to more severe responses, meaning the PTO spring terms will intensity the DWC platform heave motion, while linear damping produces less heave dynamic variations. In terms of pitch, linear damping control causes aggravate wave frequency response, so that pitch STD is increased by over 10%, while reactive control is deteriorating all the wind and wave frequency responses and the pitch resonance, which results in more vigorous pitch for DWC. On the contrary, spring-damping control is noticeably suppressing wind-induced and pitch resonance responses, leading to over 20% pitch mitigation.
3. The added WECs with different PTO control also produce insignificant influence on mooring tensions, as it is tightly coupled with platform surge motion.
4. The PTO control strategy is shown to greatly impact on the WEC power output. Reactive control leads to the highest wave power generation as expected, followed by linear damping and spring-damping control. More specifically, the absorbed wave energy from reactive control could reach 8.84%, 5.10% and 5.19% of the wind turbine power output for DCL 1-3, respectively. These values for spring-damping control, i.e. 4.54%, 3.04% and 3.10%, are almost the half. It can be noticed that the absorbed wave energy takes up a bigger portion of the wind-wave power output in below-rated condition than above-rated, which is expected to help produce great supplements for under-rated wind power output, thus largely improving the power quality of the hybrid system. At the same time, these PTO control schemes do not seem to have much influence on wind turbine power generation, the variations of which are within 1% for all DLCs.
5. The assumed optimal K_{PTO} and B_{PTO} for single DOF point absorber WECs attached to fixed structures are no logner the optimal solution for the floating hybrid power generation platform concerning both wave power production and dynamic responses.
6. In storm protection mode with WECs lifted above the water surface, symmetrical and non-symmetrical configurations have similar influence on surge and heave motion, while the average

pitch angle could possibly return to 0° in non-symmetrical mode, which is beneficial for the ultimate and fatigue loads of critical wind turbine structures, such as tower and blades.

In future study, BEM based aerodynamic load calculation and the elastic dynamics of wind turbine blades and tower could be coupled into the integrated simulation environment with FORTRAN coded DLL, in order to establish a better framework with higher fidelity and wider universality. Also note that the PTO control strategies used in this work are intentionally designed for obtaining more wave power, while not much consideration is laid on platform motion mitigation. Therefore, multi-objective design is to be further investigated both regards to WEC power increment and platform motion mitigation, by means of studying the WEC buoy number and shape, arm length, as well as more suitable PTO control strategies.

Acknowledgement

The study is supported by the National Natural Science Foundation of China (Grant No. 51705453, 51879233 and 61911530251), the Key Research and Development Program of Zhejiang Province (Grant No. 2021C03182), the Natural Science Foundation of Zhejiang Province (Grant No. LHY20E090001), the Bureau of Science and Technology of Zhoushan (Grant No. 2019C81036), and The Royal Society International Exchanges (Grant No. IEC NSFC 170294). The authors are grateful for the provision of financial support. The computational resources in the HPC Center of Zhejiang University (Zhoushan Campus) are also acknowledged.

References

[1] J. Lee, F. Zhao, Global wind report 2019, Global Wind Energy Council (2020).

[2] J. Jonkman, Dynamics modeling and loads analysis of an offshore floating wind turbine, Tech. rep., National Renewable Energy Lab.(NREL), Golden, CO (United States) (2007).

[3] B. Skaare, F. G. Nielsen, T. D. Hanson, R. Yttervik, O. Havmøller, A. Rekdal, Analysis of measurements and simulations from the hywind demo floating wind turbine, Wind Energy 18 (6) (2015) 1105–1122.

[4] D. Roddier, C. Cermelli, A. Aubault, A. Weinstein, Windfloat: A floating foundation for offshore wind turbines, Journal of renewable and sustainable energy 2 (3) (2010) 033104.

[5] T. Choisnet, E. Rogier, Y. Percher, A. Courbois, I. Crom, R. Mariani, Performance and mooring qualification in floatgen: the first french offshore wind turbine project, in: Proceedings of the 16ième Journées de l'Hydrodynamique, 2018.

[6] S. Butterfield, W. Musial, J. Jonkman, P. Sclavounos, Engineering challenges for floating offshore wind turbines, Tech. rep., National Renewable Energy Lab.(NREL), Golden, CO (2007).

[7] T. J. Larsen, T. D. Hanson, A method to avoid negative damped low frequent tower vibrations for a floating, pitch controlled wind turbine, Journal of Physics: Conference Series 75 (1) (2007) 012073.

[8] H. Namik, K. Stol, Individual blade pitch control of floating offshore wind turbines, Wind Energy 13 (1) (2010) 74–85.

[9] M. A. Lackner, M. A. Rotea, Structural control of floating wind turbines, Mechatronics 21 (4) (2011) 704–719.

[10] J. Cruz, Ocean wave energy: current status and future prespectives, Springer Science & Business Media, 2007.

[11] M. Sojo Armentia, G. Auer, Marina platform final summary report, Tech. rep., Acciona Energía, Spain (2014).

[12] L. Golman, W. Chen, E. Quevedo, E. Delory, K. Mintenbeck, J. Yu, S. Lu, The mutipurpose offshore tropos platform: Environmental and societal issues, in: Proceedings of the 2nd International Conference on Environmental Interactions of Marine Renewable Energy Technologies, Vol. 28, 2014.

[13] C. Rockmann, M. Stuiver, S. van den Burg, B. Zanuttigh, F. Zagonari, L. Airoldi, E. Angelelli, R. Suffredini, G. Franceschi, G. Belloti, et al., Multi-use platform solutions in the north sea, baltic sea, atlantic and adriatic sea: Mermaid, Tech. rep., Stichting Dienst Landbouwkundig Onderzoek (2015).

[14] F. Brennan, A. Kolios, Structural integrity considerations for the h2ocean multi modal wind-wave platform, in: Proceedings of the 2014 European Wind Energy Association Conference and Exhibition, European Wind Energy Association, 2014.

[15] C. Casale, L. Serri, N. Stolk, I. Yildiz, M. Cantù, Synergies, innovative designs and concepts for multipurpose use of conversion platforms, Tech. rep., Results of ORECCA Project–WP4 (FP7) (2012).

[16] C. Pérez-Collazo, D. Greaves, G. Iglesias, A review of combined wave and offshore wind energy, Renewable and Sustainable Energy Reviews 42 (2015) 141–153.

[17] A. Aubault, M. Alves, A. Sarmento, D. Roddier, A. Peiffer, Modeling of an oscillating water column on the floating foundation windfloat, in: Proceedings of the 30th International Conference

on Ocean, Offshore and Arctic Engineering, American Society of Mechanical Engineers, 2011, pp. 235–246.

[18] A. Peiffer, D. Roddier, A. Aubault, Design of a point absorber inside the windfloat structure, in: Proceedings of the 30th International Conference on Ocean, Offshore and Arctic Engineering, American Society of Mechanical Engineers, 2011, pp. 247–255.

[19] A. Weinstein, D. Roddier, K. Banister, Windwavefloat (wwf): Final scientific report, Tech. rep., Principle Power Inc. (2012).

[20] C. Lee, WAMIT theory manual, Massachusetts Institute of Technology, Department of Ocean Engineering, 1995.

[21] M. J. Muliawan, M. Karimirad, Z. Gao, T. Moan, Extreme responses of a combined spar-type floating wind turbine and floating wave energy converter (stc) system with survival modes, Ocean Engineering 65 (2013) 71–82.

[22] C. Michailides, Z. Gao, T. Moan, Experimental study of the functionality of a semisubmersible wind turbine combined with flap-type wave energy converters, Renewable Energy 93 (2016) 675–690.

[23] L. Wan, Z. Gao, T. Moan, Experimental and numerical study of hydrodynamic responses of a combined wind and wave energy converter concept in survival modes, Coastal Engineering 104 (2015) 151–169.

[24] Z. Gao, T. Moan, L. Wan, C. Michailides, Comparative numerical and experimental study of two combined wind and wave energy concepts, Journal of Ocean Engineering and Science 1 (1) (2016) 36–51.

[25] E. E. Bachynski, T. Moan, Point absorber design for a combined wind and wave energy converter on a tension-leg support structure, in: ASME 2013 32nd International Conference on Ocean, Offshore and Arctic Engineering, American Society of Mechanical Engineers, 2013.

[26] M. Karimirad, K. Koushan, Windwec: Combining wind and wave energy inspired by hywind and wavestar, in: Proceedings of the 2016 IEEE International Conference on Renewable Energy Research and Applications (ICRERA), IEEE, 2016, pp. 96–101.

[27] L. Li, Y. Gao, Z. Yuan, S. Day, Z. Hu, Dynamic response and power production of a floating integrated wind, wave and tidal energy system, Renewable energy 116 (2018) 412–422.

[28] Z. Cheng, T. R. Wen, M. C. Ong, K. Wang, Power performance and dynamic responses of a combined floating vertical axis wind turbine and wave energy converter concept, Energy 171 (2019) 190–204.

[29] N. Ren, Z. Ma, B. Shan, D. Ning, J. Ou, Experimental and numerical study of dynamic responses of a new combined tlp type floating wind turbine and a wave energy converter under operational conditions, Renewable Energy 151 (2020) 966–974.

[30] N. Ren, Z. Ma, T. Fan, G. Zhai, J. Ou, Experimental and numerical study of hydrodynamic responses of a new combined monopile wind turbine and a heave-type wave energy converter under typical operational conditions, Ocean Engineering 159 (2018) 1–8.

[31] M. J. Legaz, D. Coronil, P. Mayorga, J. Fernández, Study of a hybrid renewable energy platform: W2power, in: Proceedings of the 37th International Conference on Ocean, Offshore and Arctic Engineering, American Society of Mechanical Engineers Digital Collection, 2018.

[32] J. Hu, B. Zhou, C. Vogel, P. Liu, R. Willden, K. Sun, J. Zang, J. Geng, P. Jin, L. Cui, et al., Optimal design and performance analysis of a hybrid system combing a floating wind platform and wave energy converters, Applied Energy 269 (2020) 114998.

[33] W. Chen, F. Gao, X. Meng, B. Chen, A. Ren, W2p: A high-power integrated generation unit for offshore wind power and ocean wave energy, Ocean Engineering 128 (2016) 41–47.

[34] M. Kamarlouei, J. Gaspar, M. Calvario, T. Hallak, M. J. Mendes, F. Thiebaut, C. G. Soares, Experimental analysis of wave energy converters concentrically attached on a floating offshore platform, Renewable Energy 152 (2020) 1171–1185.

[35] M. Kramer, L. Marquis, P. Frigaard, et al., Performance evaluation of the wavestar prototype, in: Proceedings of the 9th European Wave and Tidal Energy Conference, Southampton, UK, Citeseer, 2011, pp. 5–9.

[36] F. d. O. António, Phase control through load control of oscillating-body wave energy converters with hydraulic pto system, Ocean Engineering 35 (3-4) (2008) 358–366.

[37] R. H. Hansen, Design and control of the power take-off system for a wave energy converter with multiple absorbers, Ph.D. thesis (2013).

[38] T. S. Hallak, J. F. Gaspar, M. Kamarlouei, M. Calvário, M. J. Mendes, F. Thiebaut, C. Guedes Soares, Numerical and experimental analysis of a hybrid wind-wave offshore floating platform's hull, in: Proceedings of the 37th International Conference on Ocean, Offshore and Arctic Engineering, American Society of Mechanical Engineers Digital Collection, 2018.

[39] H. Zhu, C. Hu, M. Sueyoshi, S. Yoshida, Integration of a semisubmersible floating wind turbine and wave energy converters: an experimental study on motion reduction, Journal of Marine Science and Technology (2019) 1–8.

[40] J. M. Jonkman, M. L. Buhl Jr, et al., Fast user's guide, National Renewable Energy Laboratory, Golden, CO, Technical Report No. NREL/EL-500-38230 (2005).

[41] A. Robertson, J. Jonkman, M. Masciola, H. Song, A. Goupee, A. Coulling, C. Luan, Definition of the semisubmersible floating system for phase ii of oc4, Tech. rep., National Renewable Energy Lab.(NREL), Golden, CO (2014).

[42] J. Jonkman, S. Butterfield, W. Musial, G. Scott, Definition of a 5-mw reference wind turbine for offshore system development, Tech. rep., National Renewable Energy Lab.(NREL), Golden, CO (2009).

[43] K. Johannessen, T. S. Meling, S. Hayer, et al., Joint distribution for wind and waves in the northern north sea, in: Proceedings of the 11th International Offshore and Polar Engineering Conference, International Society of Offshore and Polar Engineers, 2001.

[44] A. Pecher, J. P. Kofoed, Handbook of ocean wave energy, Springer London, 2017.

[45] M. J. Muliawan, M. Karimirad, T. Moan, Dynamic response and power performance of a combined spar-type floating wind turbine and coaxial floating wave energy converter, Renewable Energy 50 (2013) 47–57.

[46] A. Yde, M. M. Pedersen, S. B. Bellew, A. Køhler, R. S. Clausen, A. W. Nielsen, Experimental and theoretical analysis of a combined floating wave and wind energy conversion platform, Tech. rep., DTU Wind Energy (2014).

[47] A. ANSYS, Aqwa theory manual, ed. Canonsburg, PA 15317, USA (2013).

[48] W. Cummins, The impulse response function and ship motions, Tech. rep., David Taylor Model Basin Washington DC (1962).

[49] B. Tony, Wind energy handbook, Wiley, 2001.

[50] T. Wang, H. Jin, X. Wu, Coupled dynamic analysis of a tension leg platform floating offshore wind turbine, Journal of Offshore Mechanics and Arctic Engineering 142 (1) (2020).

[51] M. Zhou, Y. Pan, N. Ren, Y. Zhu, Operational performance of a combined tlp-type floating wind turbine and heave-type floating wave energy converter system, in: Proceedings of the 2nd International Conference on Sustainable Development, Atlantis Press, 2016.

[52] A. Babarit, Nemoh user manual, Tech. rep. (2014).

[53] G. Li, M. R. Belmont, Model predictive control of sea wave energy converters–part i: A convex approach for the case of a single device, Renewable Energy 69 (2014) 453–463.

[54] M. Lawson, Y. Yu, K. Ruehl, C. Michelen, et al., Development and demonstration of the wec-sim wave energy converter simulation tool, Tech. rep. (2014).

[55] B. J. Jonkman, M. L. Buhl Jr, Turbsim user's guide, Tech. rep., National Renewable Energy Lab.(NREL), Golden, CO (2006).

[56] S. K. Chakrabarti, Hydrodynamics of offshore structures, WIT press, 1987.

[57] M. Karimirad, T. Moan, Wave-and wind-induced dynamic response of a spar-type offshore wind turbine, Journal of waterway, port, coastal, and ocean engineering 138 (1) (2011) 9–20.

[58] Y. Han, C. Le, H. Ding, Z. Cheng, P. Zhang, Stability and dynamic response analysis of a submerged tension leg platform for offshore wind turbines, Ocean Engineering 129 (2017) 68–82.

[59] E. V. Sánchez, R. H. Hansen, M. M. Kramer, Control performance assessment and design of optimal control to harvest ocean energy, IEEE Journal of Oceanic Engineering 40 (1) (2014) 15–26.